

Authors reply to reviewer's comments:

Dear Anonymous Referees,

Thanks for your careful review of the manuscript. We read the reviewer's comments carefully, and have responded and taken all of the reviewer's comments into consideration and revised the manuscript accordingly. My detailed responses are as follows:

**Comments from Anonymous Referee #1:**

**“Major comment:**

- 1) There are two observation sites, a rural site (GC site) and an urban site (CAMS site). The Monin-Obukhov similarity theory (MOST) is applied in rural site because the surface is homogenous. But in the urban site, the observation was within the urban roughness sublayer (3-5 mean building height), MOST is invalid due to the lack of constant-flux conditions, the local similarity theory should be used. In other words, the function or the parameters in the similarity relationship should be different for the rural and urban site.”**

Response: Indeed, in the urban site (CAMS site) the observation was within the urban roughness sublayer, and the local similarity theory should be used to calculate the aerosol mass flux.

But, if the local similarity theory is applied for calculation in our experiment, the local turbulence parameters and local stability parameters are required. At the CAMS site, these parameter measurements cannot be implemented due to actual conditions. So we can only choose an alternative, and used the meteorological data (temperature) measured at nearby observation points, then based on the free convection assumption (using Equation 12) the aerosol fluxes at the CAMS site were calculated. We (Yuan et al, 2015) conducted a test experiment for vertical aerosol flux in Hefei City, China, using free convection assumptions and local similarity theories to calculate aerosol fluxes, respectively. Comparison of the calculation results of the two methods shows that very unstable condition,  $-0.15 < (z-z_d) / L < 0$ , accounts for about 62 % of the time, and the relative difference is about 5%. Under weak unstable and stable condition, the relative error is about 15%. Although the relative error is a little large under weak unstable stable stratification conditions, the absolute difference in flux is still small.

There is a weather tower in the north of Beijing. The weather tower is 6.1 km far from the CAMS site. The meteorological observation data from the weather tower show that the Monin-Oubhov similarity theory has a little significant error under stable condition, while the Monin-Oubhov similarity theory is still basically applicable in the case of unstable stratification (Liu et al. 2009). In the roughness sub-layers of other cities, under the condition of unstable stratification, the local similarity theory is similar

to MOST (Zou et al. 2018, 2019). Urban meteorological observations show that the urban surface layer is almost always in an unstable stratification. Even if the city's upper levels are stable, it is nearly always unstable near the ground in the city (Li et al., 2007). All of this shows that our current treatment is reasonable.

Please see L442-L463

#### Reference

- Li, X., Hu, F., and Shu, W.: Study on the characteristics of winter island heat islands in Beijing and the influence factors of strong and weak heat islands, *Journal of the Graduate School of the Chinese Academy of Sciences*, 4, 431-438, 2007.
- Liu Ximing, Hu Fei, Quan Lihong, Cao Xiaoyan, and Dou Junxia, 2009, Validation of the local similarity in urban boundary layer, *Climatic and Environmental Research* (in Chinese), 14(2): 183-191.
- Zou, J., Liu, G., Sun, J., Zhang, H., and Yuan, R.: The momentum flux-gradient relations derived from field measurements in the urban roughness sublayer in three cities in China, *Journal Of Geophysical Research-Atmospheres*, 120, 10.1002/2015jd023909, 2015.
- Yuan, R., Luo, T., Sun, J., Liu, H., Fu, Y., and Wang, Z.: A new method for estimating aerosol mass flux in the urban surface layer using LAS technology, *Atmospheric Measurement Techniques*, 9, 1925-1937, 10.5194/amt-9-1925-2016, 2016.
- Roth, M.: Review of atmospheric turbulence over cities, *Quarterly Journal of the Royal Meteorological Society*, 126, 941-990, 10.1256/smsqj.56408, 2000.

- 2) **“The function and parameters of the similarity relationship are not universal, the authors should explain why they use these function and parameters in the paper. For example, in Eq. 4, the authors said that they take the parameters  $b_1$  and  $b_2$  follow DeBruin et al., 1995. But in DeBruin et al., 1995, it said that “For stable conditions there is no consensus on the universal function”,  $b_1=5, b_2=0$  were found by DeBruin et al., 1993, and “the scatter was very large”. So DeBruin may not be the best choice. Especially, in Yuan et al., 2016, the parameter  $b_1$  and  $b_2$  follows Wyngaard et al., 1971., which is very different from DeBruin et al., 1993. When  $b_1$  and  $b_2$  follow DeBruin et al., 1995, it means that  $\eta(\xi)$  stays constant with stability; but when  $b_1$  and  $b_2$  follow Wyngaard et al., 1971, it means that  $\eta(\xi)$  changes constant with stability. The author should explain why they choose DeBruin et al., 1995.”**

**Response:** In addition to DeBruin et al., 1993 and 1995, there are a number of schemes that are used to parameterize the near-surface temperature structure parameter  $C_T^2$ . Available data, such as  $C_T^2$ ,  $u^*$  and  $T^*$ , were used to calculate the difference between schemes and actual data. The scheme with the smallest difference was selected.

The experiment of Yuan et al (2016) was conducted over the urban surface. The scheme of DeBruin et al (1995) was used for processing of these data for unstable

conditions, and the scheme of Wyngaard et al.(1971) was used for stable condition. When the free convection approximation is satisfied, the approximate expression given by Wyngaard et al., 1971 was used.

The current GC site is a rural site with a flat underlying surface, where similarity theory can be applied. The parameters  $T^*$  and  $u^*$  were obtained from temperature-wind profiles from a tower in GC site. After comparing several parameterization schemes, we found that taking  $b_1=5$  and  $b_2=0$  was the best match with the actual results. So we used this scheme. Details are given below.

The parameterizing scheme for the near-surface temperature structural parameter  $C_T^2$  can be expressed by the formula in the literature (Wyngaard et al., 1971), i.e.

$$\frac{C_T^2(z-d)^{2/3}}{T_*^2} = \eta\left(\frac{z-d}{L}\right) \quad (1)$$

where  $z$  is the measurement height,  $d$  is the zero-displacement height,  $\xi=(z-d)/L$  is the nondimensional stability parameter,  $L$  is the Monin-Obukhov (M-O) length and defined

as  $L = \frac{\bar{T}u_*^2}{\kappa g T_*}$ . Usually,  $\eta\left(\frac{z-d}{L}\right)$  can be,

$$\eta\left(\frac{z-d}{L}\right) = a_1 \left[1 - a_2 \frac{z-d}{L}\right]^{-2/3} \quad 0 \leq (z-d)/L \quad (2)$$

$$\eta\left(\frac{z-d}{L}\right) = b_1 \left[1 + b_2 \left(\frac{z-d}{L}\right)^{e_1}\right] \quad 0 \leq (z-d)/L \leq 2 \quad (3)$$

Five coefficients  $a_1$ ,  $a_2$ ,  $b_1$ ,  $b_2$ ,  $e_1$  in Eqs. (2) (3) were decided by different researchers, shown in Table 1.

Table1 Five coefficients in universal function

| Scheme no | $a_1$      | $a_2$      | $b_1$      | $b_2$       | $e_1$      | References  |
|-----------|------------|------------|------------|-------------|------------|---|
| <b>1</b>  | <b>4.9</b> | <b>7</b>   | <b>4.9</b> | <b>2.75</b> | <b>1</b>   | Wyngaard,1971; He_2018  |
| <b>2</b>  | <b>4.9</b> | <b>6.1</b> | <b>4.9</b> | <b>2.2</b>  | <b>2/3</b> | Andreas(1988,1989),Zhang(2015), Braam_2016, Lee_2015, Li,2017 |
| 3         | 4.9        | 7          | 6.34       | 7           | 1          | Thierrmann 等 1992   |
| <b>4</b>  | <b>4.9</b> | <b>9</b>   | <b>5</b>   | <b>0</b>    | <b>1</b>   | De Bruin 等, 1993,1995   |
| 5         | -          | -          | 4.9        | 2.4         | 2/3        | Hartogensis 等, 2005   |
| 6         | 6.1        | 7.6        |            |             |            | Maronga_2014  |
| 7         | 6.7        | 14.9       | 4.5        | 1.3         | 2/3        | Li et al.,2012  |
| 8         |            |            | 4.7        | 1.6         | 2/3        | Hartogensis,2005  |

Schemes 1, 2 and 4 were widely used, so the three were used to calculate flux for comparison in our experiment. Sensible heat flux can be calculated as,

$$H_s^i = C_p \rho u_* \sqrt{\frac{C_T^2 z^{2/3}}{\eta(z/L)}} \quad i=1,2,4, \text{ for scheme number.} \quad (4)$$

and compared with

$$H_s^0 = C_p \rho u_* T_* \quad (5)$$

The variables  $u_*$  and  $T_*$  can be obtained from 3-D sonic anemometer or temperature-wind profiles. Comparison of sensible heat flux of Eqs. (4) and (5) is equivalent to the comparison between  $\sqrt{\frac{C_T^2 z^{2/3}}{\eta(z/L)}}$  and  $T_*$  in Eq. (1)

Aerosol flux measurement was conducted in Hefei, China (Yuan et al. 2016), and  $C_T^2$  was deduced from a LAS and  $T_*$  L were deduced from an EC system. Taking  $a_1=4.9$ ,  $a_2=9$ ,  $b_1=4.9$ ,  $b_2=2.75$ , and  $e_1=0$  gives the minimal difference between Eq. (4) and Eq. (5).

For the experiment at the GC site,  $C_T^2$  was deduced from a LAS and  $T_*$  L were deduced from wind profile and temperature profile. Comparisons of sensible heat flux between  $H_s^i$  and  $H_s^0$  were done and shown in Fig. 1.

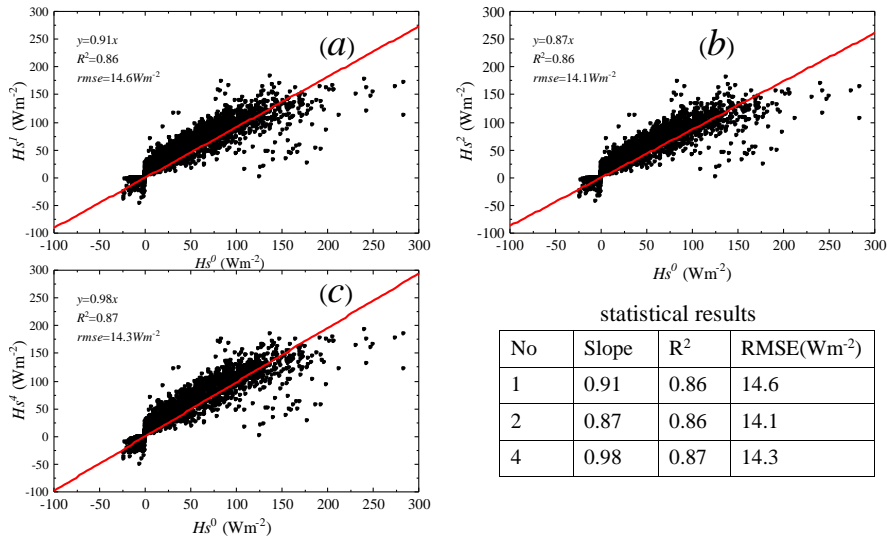


Figure 1 Comparisons between  $H_s^i$  and  $H_s^0$  (a)(b)(c) corresponding to scheme 1,2,4 respectively and statistical results are given on the lower right.

From comparisons in Fig. 1, Scheme 4 was selected to calculate flux in the current manuscript.

The effect of the footprint is not considered in our experiment.

Please see Line 194-Line 200.

#### Reference

- Andreas, E. L.: Estimating  $cn_2$  over snow and sea ice from meteorological data, *Journal of the Optical Society of America a-Optics Image Science and Vision*, 5, 481-495, 10.1364/josaa.5.000481, 1988.
- Wyngaard, J. C., Izumi, Y., and Collins, S. A.: Behavior of refractive-index-structure parameter near ground, *J. Opt. Soc. Am.*, 61, 1646-1650, 10.1364/josa.61.001646, 1971.
- DeBruin, H. A. R., vandenHurk, B., and Kohsiek, W.: The scintillation method tested over a dry vineyard area, *Boundary-Layer Meteorology*, 76, 25-40, 1995.
- Debruin, H. A. R., Kohsiek, W., and Vandenhurk, B.: A verification of some methods to determine the fluxes of momentum, sensible heat, and water-vapor using standard-deviation and structure parameter of scalar meteorological quantities, *Boundary-Layer Meteorology*, 63, 231-257, 1993.
- Andreas, E. L.: 1989, 'Two-Wavelength Method of Measuring Path-Averaged Turbulent Surface Heat Fluxes', *J. Atmos. Oceanic Tech.* 6, 280-292.
- Maronga, B.: Monin-Obukhov Similarity Functions for the Structure Parameters of Temperature and Humidity in the Unstable Surface Layer: Results from High-Resolution Large-Eddy Simulations, *Journal of the Atmospheric Sciences*, 71, 716-733, 10.1175/jas-d-13-0135.1, 2014.
- Li, D., Bou-Zeid, E., and De Bruin, H. A. R.: Monin-Obukhov Similarity Functions for the Structure Parameters of Temperature and Humidity, *Boundary-Layer Meteorology*, 145, 45-67, 10.1007/s10546-011-9660-y, 2012.
- Hartogensis, O. K., and H. A. R. De Bruin, 2005: Monin-Obukhov similarity functions of the structure parameter of temperature and turbulent kinetic energy dissipation rate in the stable boundary layer. *Bound.-Layer Meteor.*, 116, 253-276.
- Zhang, H., and Zhang, H.: Comparison of Turbulent Sensible Heat Flux Determined by Large-Aperture Scintillometer and Eddy Covariance over Urban and Suburban Areas, *Boundary-Layer Meteorology*, 154, 119-136, 10.1007/s10546-014-9965-8, 2015.
- Braam, M., Beyrich, F., Bange, J., Platis, A., Martin, S., Maronga, B., and Moene, A. F.: On the Discrepancy in Simultaneous Observations of the Structure Parameter of Temperature Using Scintillometers and Unmanned Aircraft, *Boundary-Layer Meteorology*, 158, 257-283, 10.1007/s10546-015-0086-9, 2016.
- Lee, S.-H., Lee, J.-H., and Kim, B.-Y.: Estimation of Turbulent Sensible Heat and Momentum Fluxes over a Heterogeneous Urban Area Using a Large Aperture Scintillometer, *Advances In Atmospheric Sciences*, 32, 1092-1105, 10.1007/s00376-015-4236-2, 2015.
- Thiermann, V., and Grassl, H.: The measurement of turbulent surface-layer fluxes by use of bichromatic scintillation, *Boundary-Layer Meteorology*, 58, 367-389, 10.1007/bf00120238, 1992.
- Li, X., Gao, Z., Li, Y., and Tong, B.: Comparison of Sensible Heat Fluxes Measured by a Large Aperture Scintillometer and Eddy Covariance System over a Heterogeneous Farmland in East China, *Atmosphere*, 8, 10.3390/atmos8060101,

2017.

Yuan, R., Luo, T., Sun, J., Liu, H., Fu, Y., and Wang, Z.: A new method for estimating aerosol mass flux in the urban surface layer using LAS technology, *Atmospheric Measurement Techniques*, 9, 1925-1937, 10.5194/amt-9-1925-2016, 2016.

- 3) **“In L359 The conventional meteorological parameters were measured at 20m above the ground surface. But in L275, the author said that the measurement heights of temperature and wind speed were 1.5 m and 10 m at CAMS site (Beijing). It should be clear which data were used to calculate the aerosol flux. Because the average height of the building was 24m in CAMS site, and LAS was located at 43meters. The temperature measured at 1.5m within the canopy layer is different from 43m above the canopy layer, and the calculation of aerosol fluxes from Eq. 12 was badly influenced.”**

Response: There are a few errors in depicting measurement height. The conventional meteorological parameters are measured on the same roof, 20 meters away from the receiving end and in the northwest direction of the receiving end. The measurement heights were 1.5 m and 10 m above the roof for air temperature and wind speed. Please see L336-L339.

- 4) **“Another issue that the authors need to address is the assumption between AERI( atmospheric equivalent refractive index) and aerosol mass concentration as well as aerosol adsorption. First, there do exist some light-absorbing trace gases in the atmosphere, which may influence AERI significantly. Second, aerosol absorption generally contributes a relatively small part of the extinction. By contrast, scattering components like sulfate and organic matters dominate aerosol extinction during haze pollution episode, especially under high humidity. Last but not at least, aerosol extinction is also closely related to the number concentration and size distribution, which need to be considered here. I do not think it is technically robust to simply get the relationship between the imaginary part of the AERI and the atmospheric aerosol mass concentration in Eq.6.”**

Response: The light wavelength is 0.620  $\mu\text{m}$ . This wavelength is only weakly absorbed by O<sub>3</sub>; therefore, the observed absorption is primarily due to aerosol (Brion et al., 1998; Lou et al., 2014; Nebuloni, 2005).

Aerosol extinction is also closely related to the number concentration, size distribution, and refractive index of aerosol particles, so there is not a simple linear relationship between the imaginary part of the AERI and the atmospheric aerosol mass concentration in Eq.6. The variations in the ratio of the aerosol mass concentration to the imaginary part of the AERI will introduce errors into the aerosol mass flux

measurements.  $R_{MN}$  should be obtained by simultaneously measuring  $M_a$  and the imaginary part of the AERI at the same location with the LAS so that real-time  $R_{MN}$  can be obtained.

For GC site and CAMS site, measuring positions of  $PM_{10}$  and visibility are a little far from LAS measurement. So a constant ratio  $R_{MN}$  is more representative than a simultaneous value.

Our experiment conducted in Hefei (Yuan et al. 2016) showed that the linear correlation coefficient between  $PM_{10}$  and the imaginary part of the AERI is 0.94. This indicates that constant is a reasonable assumption for a given location with a dominant aerosol type, such as urban aerosols. Of course, when measurements for aerosol flux using a LAS,  $PM_{10}$  and visibility are performed together, simultaneous value for  $R_{MN}$  is better.

Please see L234-L236 and L408-L422.

Reference:

Brion, J., Chakir, A., Charbonnier, J., Daumont, D., Parisse, C., and Malicet, J.: Absorption spectra measurements for the ozone molecule in the 350-830 nm region, *J. Atmos. Chem.*, 30, 291-299, 10.1023/a:1006036924364, 1998.

Lou, S., Liao, H., and Zhu, B.: Impacts of aerosols on surface-layer ozone concentrations in China through heterogeneous reactions and changes in photolysis rates, *Atmos. Environ.*, 85, 123-138, 10.1016/j.atmosenv.2013.12.004, 2014.

Nebuloni, R.: Empirical relationships between extinction coefficient and visibility in fog, *Appl. Opt.*, 44, 3795-3804, 10.1364/ao.44.003795, 2005.

Yuan, R., Luo, T., Sun, J., Liu, H., Fu, Y., and Wang, Z.: A new method for estimating aerosol mass flux in the urban surface layer using LAS technology, *Atmospheric Measurement Techniques*, 9, 1925-1937, 10.5194/amt-9-1925-2016, 2016.

**“Minor issues: Some statements in this manuscript are very hard to follow. Language editing is needed for improving the accuracy of language as well as overall readability.”**

Response: We’ve tried our best to improve the English writing in the revised manuscript, but also a native English speaker reviewed the revised version of the manuscript.

**1) “Line 43: Please rephrase ‘heavy pollution weather’”**

Response: heavy pollution environment

Please see Line 45-46.

**2) “Line 48: ‘few studies’ should be ‘few study’”**

Response: We modified it.

**3) “Line 72: what is the boundary layer box model? Usually box model is zero-dimensional.”**

Response: The boundary layer box model means the boundary layer is taken as a box. The box is filled within duration  $\tau$  with flux  $F$ , and then flux  $F$  can be estimated by the boundary layer box model:

$$F = C * H_{BL} / \tau$$

where  $C$  was the concentration measured at 30 m height,  $H_{BL}$  was the measured boundary layer height averaged over the sample duration, and  $\tau$  was boundary layer filling time.

More details is in Ceburnis et al. (2016).

I add an explanation. Please see Line 77-78.

Reference:

Ceburnis, D., Rinaldi, M., Ovadnevaite, J., Martucci, G., Giulianelli, L., and O'Dowd, C. D.: Marine submicron aerosol gradients, sources and sinks, *Atmospheric Chemistry and Physics*, 16, 12425-12439, 10.5194/acp-16-12425-2016, 2016.

**4) “Line 106: should be ‘makes it possible’”**

Response: We modified it in Line 113.

**5) “Eq. 11: replace  $z$  with  $(z-d)$ ”**

Response: We modified it. Please see Line 276.

**6) “Line 304: More detail needed, not “personal experience.””**

Response: We specified personal experience as “trend comparison for same variables between different heights and different locations.” Please see L367-368.

**7) “Line 378: weakly unstable is not free convection. The free convection**



**assumption was not satisfied at night.”**

Response: When the free convection assumption is applied to weakly unstable condition at night, the assumption will result in an some uncertainty. In many cases, similar to the LAS-derived sensible heat flux, we can only choose free convection assumption to obtain flux. Under stable conditions or weakly unstable condition, the value of the flux data is small and does not cause significant error. Of course, a better approach is to get  $u^*$  and  $T^*$  from meteorological variable and calculate aerosol flux according to Eq. (10). Please see L445-451.

**Comments from Anonymous Referee #2:**

**“Quantification of the aerosol mass flux is an important topic to understand pollutant emissions and transport over areas exposed to pollution episodes. The study utilizes an innovative large aperture scintillometer (LAS) technique to estimate the transport of aerosols over extended areas. The presented results are a valuable contribution to the understanding the emissions in urban areas and rural polluted regions.”**

- 1) “However, since the LAS technique is semi-empirical, then additional information on testing and evaluation of such measurements would help to improve confidence in results and understand the underlying uncertainties. For example, the LAS technique is capable to determine the magnitude of the flux but not the sign. In general the aerosols are very heterogeneous in space and the measured fluxes show typically large variation in magnitude including the sign. Over the polluted areas, which behave as the source, the emissions presumable overwhelmingly exceed the deposition sinks. Therefore, for example, a rough quantification of the deposition sink would allow to conclude that the sink term is indeed negligible and the flux quantified by LAS can be safely assumed to represent the upward fluxes. If available, the reference to comparison of the LAS method results with a more direct micrometeorological measurement would be very useful (if this was done in Yuan et al., 2016, please mention explicitly).”**

Response: Thanks for your suggestion.

We have added the statement that the sink term is indeed negligible and the flux quantified by LAS can be assumed to represent the upward fluxes.

Please see L288-290.

At present, we have not conducted more direct meteorological measurements to obtain aerosol fluxes, such as the use of EC methods for aerosol flux measurements. Next, we will compare the aerosol flux obtained by LAS with the aerosol flux received by the EC method.

- 2) **“The manuscript would benefit also from better improved description/definition of the heavy pollution episodes (HPEs), how they are divided into stages of transport (transport stage TS), a cumulative stage (CS) and a removal stage (RS), and in particular what are the prevailing meteorological and aerosol emission/transport conditions during such episodes. This would help readers who are not familiar with HPE mechanisms more easily to follow the manuscript.”**

Response: Based on meteorological causes of the increase or decrease in PM<sub>2.5</sub> mass concentrations, the HPEs are divided into TSs, ASs (in the new version, CS denoted as AS by suggestion), and RSs. During the TSs, the PM<sub>2.5</sub> is dominated by relatively strong southerly winds, which carry polluted air masses from more populated southern industrial regions (Guo et al., 2014; Zhong et al., 2018a). Before rising processes during TSs, the urban PM<sub>2.5</sub> mass concentration of Baoding, which is typically representative of pollution conditions in the south of Beijing, was much higher than Beijing; the winds in Beijing rapidly shifted from northerly to southerly. Then the rising in PM<sub>2.5</sub> occurred, consistently with southerly slight or gentle breezes in the BL. The southerly air mass moves more than 288 km d<sup>-1</sup> below 500 m (estimated from the measured wind speed), which are fast enough to transport pollutants to Beijing. Such processes indicate southerly pollutant transport is primarily responsible for the rising, given the pollution transport pathway of the southwest wind belt determined by the unique geographic features of the North China Plain, with the Tai-hang Mountains and the Yan Mountains strengthening the southwest wind belt and leading the convergence of pollutant transport in Beijing (Su et al., 2004). During the ASs, PM<sub>2.5</sub> increase is dominated by stable atmospheric stratification characteristic of southerly slight or calm winds, near-ground anomalous inversion, and moisture accumulation. When the vertical aerosols are accumulated to a certain degree, the dominant scattering aerosols will substantially back-scatter solar radiation, causing a reduction in the amount of solar radiation that reaches the surface, which creates a near-ground cooling effect through atmospheric circulation and vertical mixing (Zhong et al., 2018b). The temperature reduction induces or reinforces an inversion that further weakens turbulence diffusion and results in a lower BL height, which further worsens aerosol pollution. This condition also decreases the near-ground saturation vapor pressure and suppresses water vapor diffusion to increase the relative humidity (RH), which will further enhances aerosol hygroscopic growth and accelerates liquid-phase and heterogeneous reactions to worsen aerosol pollution (Ervens et al., 2011; Kuang et al., 2016; Pilinis et al., 1989; Zhong et al., 2018a; Zhong et al., 2018b). This feedback effect of further worsened meteorological conditions aggravates PM<sub>2.5</sub> pollution (Zhong et al., 2017). During the RSs, strong northwesterly winds whose velocity increases with height occur mostly. Strong northerly winds are from less populated north mountainous areas and carry unpolluted air masses to Beijing, which is favorable for pollution dispersion.

We have added some descriptions about three stages in the introduction. Please L135-156 in Section introduction.

- Ervens, B., Turpin, B.J., Weber, R.J., Secondary organic aerosol formation in cloud droplets and aqueous particles (aqSOA): a review of laboratory, field and model studies, *Atmos. Chem. Phys.* **11**(2011), 11069-11102.
- Guo, S. *et al.*, Elucidating severe urban haze formation in China, *Proc. Natl. Acad. Sci. U.S.A.* **111**(2014), 17373-17378.
- Kuang, Y., Zhao, C.S., Tao, J.C., Bian, Y.X., Ma, N., Impact of aerosol hygroscopic growth on the direct aerosol radiative effect in summer on North China Plain, *Atmospheric Environment* **147**(2016), 224-233.
- Pilinis, C., Seinfeld, J.H., Grosjean, D., Water content of atmospheric aerosols, *Atmos. Environ.* **23**(1989), 1601-1606.
- Su, F., Gao, Q., Zhang, Z., REN, Z.-h., YANG, X.-x., Transport pathways of pollutants from outside in atmosphere boundary layer, *Res. Environ. Sci.* **1**(2004), 26-29.
- Zhong, J. *et al.*, Feedback effects of boundary-layer meteorological factors on cumulative explosive growth of PM<sub>2.5</sub> during winter heavy pollution episodes in Beijing from 2013 to 2016, *Atmos. Chem. Phys.* **18**(2018a), 247-258.
- Zhong, J., Zhang, X., Wang, Y., Liu, C., Dong, Y., Heavy aerosol pollution episodes in winter Beijing enhanced by radiative cooling effects of aerosols, *Atmos. Res.* **209**(2018b), 59-64.
- Zhong, J. *et al.*, Relative contributions of boundary-layer meteorological factors to the explosive growth of PM 2.5 during the red-alert heavy pollution episodes in Beijing in December 2016, *J. Meteorolog. Res.* **31**(2017), 809-819.

- 3) **“According the author the TS is the period when the pollution over the measurement location was mainly contributed by the downwind pollution sources. But presumable also the local sources were also a significant contribution because the aerosol fluxes did not differ much in magnitude from subsequent phases. The CS (perhaps would be better to call accumulation stage?) represents the period of rapid accumulation of pollutants and it is not evident of this occurs because of downwind transport of pollutants trapped in the atmospheric boundary layer or local emissions or both. Therefore, it is not clear if the stage differs from the TS in terms of location of emission sources or difference is made by the meteorological conditions favouring accumulation of the pollutants in the ABL. Regarding the RS, presumably the pollutant concentrations drop due to the atmospheric mixing and transport to higher levels. The other possibility is removal by scavenging or dry deposition. Dry deposition however is a slow process and also the results do not support such assumption (up-ward fluxes in Figs. 5 and 6 during the RS). ”**

Response: After a series of measures and actions, including air pollutant emission reduction, energy structure adjustments to decrease the dependence on fossil fuels, and other supportive policies, the emission sources in Beijing are strikingly less than the polluted southern industrial regions with large anthropogenic emissions. Therefore, the contribution of local emissions in Beijing is relatively smaller than that in the other

areas such as Baoding.

The TS will appear before CS. The south or southwest wind will always appear in the TS, and the concentration of PM<sub>10</sub> in Baoding is higher than the concentration of PM<sub>10</sub> in Beijing, which is generally maintained for one to two days.

Except for the southerly or southwesterly winds for one to two days, there will be no CS in Beijing. Even if it is a southerly or southwesterly wind, if the wind speed is too small ( $<1\text{ms}^{-1}$ ), AS will not appear. Only the southerly or southwesterly wind with a wind speed higher than a specific value ( $>1.5\text{ms}^{-1}$ ), and the concentration of PM<sub>2.5</sub> in the area to the south of Beijing is higher than that in Beijing, and then there will be CS after a small wind.

Therefore, the main reason for the explosive growth of aerosol concentration during CS is that explosive growth is attributed to the horizontal transport during TS.

Please L591-603.

- 4) **“The explanation in l. 425 is confusing as if the particles are removed from the atmosphere and reduction in pollutants does not occur because of the atmospheric mixing (and upward transport of aerosols). “**

Response: We modified the expression.

During the RSs, strong northwesterly winds whose velocity increases with height occur mostly. Strong northerly winds are from less populated north mountainous areas and carry unpolluted air masses to Beijing, which is favorable for pollution dispersion.

Please L154-157.

- 5) **“In relation to interaction between the aerosol pollution and meteorology, the authors suggest in the abstract (and l. 498-500) that the aerosol pollution had an effect to turbulence intensity leading to further weakening of mixing and increased accumulation. Such effect is not directly evidenced by the results in the manuscript (or cannot be distinguished) and should be further supported by the literature references rather than stated as the result.”**

Response: Based on the results in the manuscript, the effect of the aerosol pollution cannot be drawn out to turbulence intensity leading to further weakening of mixing and increased accumulation.

Based on our measurement, it can be seen that from the TS to the AS, the aerosol vertical turbulent flux decreased, but the aerosol particle concentration within surface layer increased, and it is inferred that in addition to the contribution of regional transport from upwind pollution areas during the TS, suppression of vertical turbulence mixing confining aerosols to a shallower boundary layer increased accumulation.

We modified some expression. Please see L580-584.

**“The manuscript would benefit also from numerous minor improvements**

and language editing. Please see my specific comments below.”

### **Specific comments**

- 1) **“Line 28-29, sentence difficult to follow, please revise.”**

Response: The sentence means a weakened turbulence intensity and low vertical aerosol fluxes in winter and polluted areas such as GC

We revised. Please see L28-29.

- 2) **“L. 35-36, the statement is vague, see also general comments.”**

Response: The sentence is just a reference, not a conclusion. So the sentence is deleted.

- 3) **“L. 60-61 “the consumption of a product” – revise phrasing”**

Response: expressed as “product energy consumption”. Please Line 62-63.

- 4) **“L. 77-79: the EC method has been used already for decades to quantify the aerosol particle number fluxes. As an example of earlier studies, see e.g. Buzorius, G., Rannik, Ü., Mäkelä, J.M., Vesala, T., Kulmala, M., 1998. Vertical Aerosol particle fluxes measured by eddy covariance technique using condensational particle counter. J. Aerosol Sci., 29, 157-171.”**

Response: The manuscript was revised according to the comment. Please see line 86-87.

- 5) **“L. 80, The EC method enables to determine the vertical turbulent flux, which can be different from total vertical transport. Also, the flux is provided by the cross-covariance (and not correlation).”**

Response: “eddy correlation” modified to “eddy covariance”

- 6) **“L. 82-83, the EC principle allows to quantify the number flux from fluctuation measurements, rephrase the sentence.”**

Response: Based on EC principle, the vertical velocity fluctuations and the fluctuations

in the aerosol particle number density can be measured, and the EC principle allows to quantify the number flux from fluctuation measurements.

We modified the sentences. Please see Line 88-89.

- 7) **“L. 105, The eddy correlation principles have been widely used (or something like this, revise the sentence).”**

Response: “eddy correlation” modified to “eddy covariance.”

- 8) **“L. 126 how much the surface emissions contribute to the concentration of pollutants”**

Response: At present, the question cannot be answered. We hope that with the measurement of the near-surface aerosol vertical flux, the results will help understand the accumulation of local aerosol concentrations, how much the surface emissions contribute to the level of pollutants, and how much the concentration of pollutants is attributed to upwind areas. This article does not discuss this issue for the time being. We will combine the data from the lidar and present it in a later article.

- 9) **“L. 142-143, phrasing is not good. Rather the transport properties or the statistical aerosol transport is similar to that of scalars? In fine detail the aerosol motion can be different from the air motion and the statement is not strictly correct.”**

Response: The spectral characteristics of aerosol number concentration fluctuations approximate the spectral characteristics of molecular density fluctuations.

Please see Line 175-176.

- 10) **“L. 166-167, temperature is not a passive atmospheric constituent because buoyancy affects strongly the motion of air. Also “distribution” does not seem relevant but maybe just “small particles”. Rather say that similarity of atmospheric aerosols and temperature can be assumed for the purpose.”**

Response: You are very kind and helpful for the manuscript. Please see Line 206-207.

- 11) **“L. 173 “aerosol particles are continuously dispersed in the air”, the meaning and purpose of this sentence is not clear.”**

Response: Although the aerosol particles are dispersed in the air, the macroscopic behavior of the gas-particle two-phase mixture is the same as if it is perfectly continuous in structure and physical quantities, such as the mass and refractive index associated with the matter contained within a given small volume, which will be regarded as being spread continuously over that volume.

We modified the manuscript. Please see Line 213-216.

**12) “L. 192, Correct  $R_{\{MN\}}$ ”**

Response: We Modified it.

**13) “L. 209-212, please provide reference and/or explanation for the relation between the high/low frequency fluctuations and the real/imaginary parts of the AERI.”**

Response:  $C_{n,Re}^2$  and  $C_{n,Im}^2$  can be measured by a specially made LAS (Yuan et al., 2015).

After a spherical wave propagates over a distance in a turbulent atmosphere, the light intensity on the receiving end will fluctuate. When the attenuation caused by scattering and absorption along the propagation path is very weak, light intensity fluctuation depends on the variation of the real part of the AERI along the propagation path. When the attenuation caused by scattering and absorption along the propagation path is relatively strong, the light intensity fluctuation is also related to the fluctuation of the imaginary part of the AERI along the propagation path. With the spectral analysis method, the LAS light intensity fluctuations can be separated into the contributions of the real and imaginary parts of the AERI. The input of the real part of the AERI corresponds to the high frequencies, whereas the participation of the imaginary part of the AERI corresponds to the low frequencies, suggesting that the variances resulting from the real and imaginary parts are independent. Therefore, the light intensity variances induced by the real and imaginary parts can be detected separately at high frequencies and low frequencies from the LAS measurements (Yuan et al. 2015).

We added the explanation. Please Line 257-271.

**14) “L. 225, turbulent fluctuations of what?”**

Response: Temperature

**15) “L. 297, e.g. stands for “for example”, not relevant here.”**

Response: Namely

**16) “L. 309-310. The method for judging.. sentence difficult to follow, rephrase.”**

Response: The 6-point moving average is done for the trend.

**17) “L. 315, how was “mean of the adjacent difference” defined, based on the moving average or how? Improve wording of the sentence.”**

Response: The difference between adjacent moments is denoted and abbreviated as AMD. We have modified the sentences.

We modified the paragraph. Please Line 373-385.

**18) “L. 321-321, is the exact shape of the spectrum relevant? Or the method relies purely on the Kolmogorov’s power laws of the spectra?”**

Response: The theoretical expression for the relation between light scintillation and the structure parameter are based on von Karman spectrum. It is assumed that the actual turbulence is accord with von Karman spectrum, and then the parameters are calculated. The deviation from the assumption will cause the error.

We modified the sentence. Please see Line 619-620.

**19) “L. 328, “heavy pollution weather conditions “is a bit weird, please rephrase”**

Response: under heavy pollution weather conditions modified as during heavy pollution episodes (HPEs). Please see Line 397.

**20) “L. 361, rather the wind direction varied throughout day? there was no dominant wind direction”**



Response: The wind direction has diurnal variation characteristics, which are related to the sea-land breeze, valley wind and urban heat island circulation which may exist under the control of weak weather system.

Please see Line 433-435.

**21) “L. 368-374. The “free convection” conditions are not always easily satisfied. Free convection means that the buoyancy-driven turbulence dominates over mechanical turbulence and this is not just the unstable conditions but the free convective limit of the unstable conditions. Please clarify and evaluate the uncertainties introduced by such assumption.”**

Response: At the CAMS site, local turbulence and local stability parameter measurements cannot be implemented. So we can only choose an alternative, and used the meteorological data (temperature) measured at nearby observation points, then based on the free convection assumption (using Equ. 12) the aerosol fluxes at the CAMS site were calculated. We (Yuan et al, 2015) conducted a test experiment for vertical aerosol flux in Hefei City, China, using free convection assumptions and local similarity theories to calculate aerosol fluxes. Comparison of the calculation results of the two methods shows that precarious condition,  $-0.15 < (z-z_d) / L < 0$ , accounts for about 62 % of the time, and the relative difference is about 5%. Under weak unstable and stable condition, the relative error is about 15%. Although the relative error is a little significant under weak unstable stable stratification conditions, the absolute difference in flux is still small.

We added some explanation. Please see L445-451.

**22) “L. 421, southerly wind conditions”**

Response: southerly wind

**23) “Figures 3-6, the square value of the structure parameter is plotted according to label in y-axis of the relevant subplots.”**

Response: Regarding the naming of  $C_n$  and  $C_n^2$ , I checked it. In the book of Monin and Yaglom (1975) and the book of Tatarskii (1961), there is no name for  $C_n$  and  $C_n^2$ . In later books, different books have different names. For example, in Ishimaru (1978),  $C_n$  is called a structure parameter, and  $C_n^2$  is also called a structure parameter. In Andrews and Phillip (2005),  $C_n^2$  is called a structural parameter. Considering that we have always called  $C_n^2$  as a structural parameter (Yuan et al., 2015; Yuan et al. 2016), and in the

application of  $C_n^2$  it generally appears in the form of  $C_n^2$ , I will refer to  $C_n^2$  as a structural parameter in this manuscript.

Andrews, L. C., and Phillips, R. L.: Laser beam propagation through random media, SPIE, 2005.

Monin, A. S., and Yaglom, A. M.: Statistical fluid mechanics: Mechanics of turbulence, MIT Press, Cambridge, Massachusetts, 874 pp., 1975.

Ishimaru, A.: Wave propagation and scattering in random media, Oxford University Press, Walton Street, Oxford OX2 6DP, 590 pp., 1978.

Tatarskii, V. I.: Wave Propagation in a Turbulent Medium, McGraw-Hill Book Company Inc., New York, 285 pp., 1961.

Yuan, R., Luo, T., Sun, J., Liu, H., Fu, Y., and Wang, Z.: A new method for estimating aerosol mass flux in the urban surface layer using LAS technology, Atmospheric Measurement Techniques, 9, 1925-1937, 10.5194/amt-9-1925-2016, 2016.

Yuan, R., Luo, T., Sun, J., Zeng, Z., Ge, C., and Fu, Y.: A new method for measuring the imaginary part of the atmospheric refractive index structure parameter in the urban surface layer, Atmospheric Chemistry and Physics, 15, 2521-2531, 10.5194/acp-15-2521-2015, 2015.

**24) “Discussion and conclusions: how do the measured aerosol mass-fluxes compare with relevant literature values and/or earlier measurements and typical emission estimates? Please discuss this how to results contribute to understanding of pollution emissions.”**

Response: Compared to the results (Yuan et al. 2016) from Hefei, China, a small and medium-sized provincial capital city in East China, the measured aerosol mass-fluxes in Beijing are almost at the same amount. A series of measures and actions have been made for emission reduction in Beijing, and the primary emission is from vehicles. The difference in aerosol mass flux may be small.

We added some discussion. Please Line 604-607.

Finally, the authors thank the two referees for their constructive comments that help us to improve the clarity and the quality of the manuscript greatly. All the comments are answered and the modifications introduced in the revised manuscript correspondingly. We sincerely hope our answers can relieve doubts and give a better description of our work.

# Aerosol Vertical Mass Flux Measurements During Heavy Aerosol Pollution Episodes at a Rural Site and an Urban Site in the Beijing Area of the North China Plain

Renmin Yuan<sup>1</sup>, Xiaoye Zhang<sup>2,4</sup>, Hao Liu<sup>1</sup>, Yu Gui<sup>1</sup>, Bohao Shao<sup>1</sup>, ~~Xiaoping~~Xiaoping Tao<sup>5</sup>, Yaqiang Wang<sup>2</sup>, Junting Zhong<sup>2</sup>, Yubin Li<sup>3</sup> and Zhiqiu Gao<sup>3</sup>

<sup>1</sup>School of Earth and Space Sciences, University of Science and Technology of China, Anhui, 230026, China

<sup>2</sup>State Key Laboratory of Severe Weather & Key Laboratory of Atmospheric Chemistry of CMA, Chinese Academy of Meteorological Sciences, Beijing 100081, China

<sup>3</sup>School of Geography and Remote Sensing, Nanjing University of Information Science and Technology, Nanjing 210044, China

<sup>4</sup>Center for Excellence in Regional Atmospheric Environment, IUE, CAS, Xiamen 361021, China.

<sup>5</sup>School of Physical Sciences, University of Science and Technology of China, Anhui, 230026, China.

Correspondence: Renmin Yuan (rmyuan@ustc.edu.cn) and Xiaoye Zhang (xiaoye@cma.gov.cn)

## Abstract:

Due to excessive anthropogenic emissions, heavy aerosol pollution episodes (HPEs) often occur during winter in the Beijing-Tianjin-Hebei (BTH) area of the North China Plain. Extensive observational studies have been carried out to understand the causes of HPEs; however, few measurements of ~~aerosol~~-vertical ~~aerosol~~ fluxes exist, despite them being the key to understanding vertical aerosol mixing, specifically during weak turbulence stages in HPEs. In the winter of 2016 and the spring of 2017, ~~based on the light propagation theory and surface-layer similarity theory,~~ aerosol vertical mass fluxes were measured by combining large aperture scintillometer (LAS) observations, surface PM<sub>2.5</sub> and PM<sub>10</sub> mass concentrations, and meteorological observations, including temperature, relative humidity (RH), and visibility, at a rural site in Gucheng (GC), Hebei Province, and an urban site at the Chinese Academy of Meteorological Sciences (CAMS) in Beijing located 100 km to the northeast. ~~These are based on the light propagation theory and surface-layer similarity theory.~~ The near-ground aerosol mass flux was generally lower in winter than in spring and weaker in rural GC than in urban Beijing. This finding provides direct observational evidence ~~from the perspective of vertical aerosol fluxes~~ for a weakened turbulence intensity ~~and low vertical aerosol fluxes~~ in winter and ~~in~~ polluted areas such as GC. The HPEs included a transport stage (TS), an accumulative stage (AS), and a removal stage (RS). During the HPEs from ~~25~~ January ~~25~~, 2017 to January 31, 2017, in Beijing, the mean mass flux decreased by 51% from 0.0049 mg m<sup>-2</sup>s<sup>-1</sup> in RSs to 0.0024 mg m<sup>-2</sup>s<sup>-1</sup> in the TSs. During the ASs, the mean mass flux decreased further to 0.00087 mg m<sup>-2</sup>s<sup>-1</sup>, accounting for approximately 1/3 of the flux in the TSs. A similar reduction from the TSs to ASs was observed in the HPE from ~~16~~ December ~~16~~, 2016 to ~~22~~ December ~~22~~, 2016 in GC. ~~The weakened mass flux indicates~~It can be seen that ~~from the already weak turbulence would be further weakened by TS to the AS, the~~ aerosol pollution to a certain extent, which would further

带格式的：字体：Times New Roman

带格式的：无孤行控制

带格式的：字体颜色：自动设置

带格式的：字体颜色：自动设置

带格式的：字体颜色：自动设置

facilitate vertical turbulent flux decreased, but the aerosol particle concentration with surface layer increased, and it is inferred that in addition to the contribution of regional transport from upwind areas during the TS, suppression of vertical turbulence mixing confining aerosols to a shallow boundary layer increased accumulation.

带格式的: 字体颜色: 自动设置

带格式的: 字体颜色: 自动设置

带格式的: 字体颜色: 红色

## 1 Introduction

Recently, due to the country's rapid development of industrialization and urbanization, China has experienced heavy aerosol pollution episodes (HPEs), particularly in the Beijing, Tianjin and Hebei (BTH) region, which is one of the most polluted areas in China (Zhang et al., 2012; Zhang et al., 2012). The HPEs pollution episodes often last for a long duration in the BTH region and cover a wide area, particularly in winter; they also severely reduce near-ground visibility (Lei and Wuebbles, 2013; Lei and Wuebbles, 2013) and can have detrimental effects on public health (He et al., 2018; Cao et al., 2012; He et al., 2018; Cao et al., 2012). This heavy pollution weather environment has received extensive attention in recent years, and many observational studies have been carried out (Zhong et al., 2018a; Sun et al., 2014; Wang et al., 2015; Guo et al., 2011; Zhang et al., 2009b; Huang et al., 2014; Zhong et al., 2018b; Sun et al., 2014; Wang et al., 2015; Guo et al., 2011; Zhang et al., 2009b; Huang et al., 2014). Modelling studies have also been performed to examine the regional transport of pollutants (Wang et al., 2014; Wang et al., 2014) and to study the important role of large-eddy convective turbulent mixing in the vertical transfer of pollutants from a field campaign in Beijing (Li et al., 2018; Li et al., 2018). However, few studies study on the turbulence contribution of the aerosol transport turbulent flux in the surface layer have been conducted.

Ground pollutant emissions are known as the main source of aerosols in the atmosphere. However, in previous studies, no measurements of ground emissions during heavy pollution events were collected. Surface emission data are currently required for model verification and pollution predictions, and these data are primarily obtained through emission inventories (Wu et al., 2012; Wu et al., 2012; Bond et al., 2004). The establishment of emission inventories is primarily based on emission activity and emission factor (EF) data (Akagi et al., 2011; Lu et al., 2011; Roden et al., 2006; Zhang and Tao, 2009; Akagi et al., 2011; Lu et al., 2011; Roden et al., 2006; Zhang and Tao, 2009). Emissions data are mainly obtained from statistical yearbooks (Zhang et al., 2009a; Zhang et al., 2009a). Some studies have used fixed EFs while others have implemented dynamic EFs (Bond et al., 2004; Zhang et al., 2009a; Zhang et al., 2009a). Many factors are considered in dynamic EFs, such as the size of a city, the degree of economic development, the type of fuel, the type kind of technology, the product energy consumption of a product, the control technology, and so on, as well as estimates based on actual measured meteorological parameters and aerosol parameters (Chen et al., 2015; Karvosenoja et al., 2008; Shen et al., 2013; Chen et al., 2015; Karvosenoja et al., 2008; Shen et al., 2013). A numerical model has also been used to estimate average fleet emission factors in typical urban conditions (Ketzel et al., 2003; Krecl et al., 2018; Ketzel et al., 2003; Krecl et al., 2018). The error in aerosol fluxes based on the use of emission inventories is very large (Liu et al., 2017; Zheng et al., 2017). The uncertainties in the emissions of primary aerosols for inventories are much high due to the highly uncertain contributions from the residential sector (Li et al., 2017), and the error in aerosol fluxes based on the use of emission inventories is huge (Liu et al., 2017; Zheng et al., 2017). Emission inventories constructed using the EF method provide only the total emission amount of atmospheric pollutants within a region. However, the emission data should be gridded to

a suitable scale for air quality ~~modelling~~ modeling and pollution predictions. Thus, near-surface aerosol emission data with a higher temporal and spatial resolution are urgently needed.

Many methods have been used to obtain aerosol flux data. For the upward transport of aerosols near the surface layer, the aerodynamic ~~method~~ approach was adopted in the early years, and the aerosol concentration gradient at different heights was measured and then calculated based on the similarity theory of the near-surface layer or calculated by the boundary layer box model, which can be based on meteorological data and the boundary layer is taken as a box (Ceburnis et al., 2016; Hourdin et al., 2015; Zhang and Li, 2014) (Ceburnis et al., 2016; Hourdin et al., 2015; Zhang and Li, 2014). The emission rates of bioaerosols were also estimated from spore counts and molecular tracers (Elbert et al., 2007) (Elbert et al., 2007). The abundance of microbes and meteorological data were measured, and an estimate may be derived ~~off~~ from the sea-air exchange of microorganisms (Mayol et al., 2014) (Mayol et al., 2014).

With the use of instruments for measuring the number of aerosol particles during recent years (for example, the GP-WCPC3787 particle counter by TSI), the eddy covariance (EC) method has been applied, and measurements of the aerosol particle number flux have become possible. The vertical transport flux of the aerosol particle number density  $F_p$  is denoted as a cross-correlation between the aerosol particle number concentration  $N'$  and the vertical wind speed  $w'$  (Ripamonti et al., 2013). Based on this principle, the vertical velocity fluctuations and the fluctuations in the aerosol particle number density can be measured. As a result, the vertical transport flux of the aerosol particle number density has been measured in many cities, such as in Toronto, Canada (Gordon et al., 2011), Stockholm, Sweden (Vogt et al., 2011b), Helsinki, Finland (Ripamonti et al., 2013), London, UK (Harrison et al., 2012), the Blodgett Forest Observatory in the United States (Farmer et al., 2011), and measurements of sea salt aerosol fluxes in northern Europe (Brooks et al., 2009; Sproson et al., 2013). These results have shown the quantitative relationship among urban aerosol fluxes, urban vehicle emissions, and meteorological conditions (Jarvi et al., 2009) and have been used to determine sea salt aerosol transport characteristics and provide further knowledge of aerosol properties (Nemitz et al., 2009). These measurements have been mainly collected in cities because of their anthropogenic contributions to aerosol emissions. These data can be used as routine model inputs. Direct eddy covariance measurements of aerosol exchanges in tropical forests, where primary biological aerosol particles represent a substantial fraction of the airborne particulate matter (Graham et al., 2003), were also performed by Ahlm et al. (2010a and 2010b) and Whitehead et al. (2010), potentially giving a proxy for microbial emissions in tropical ecosystems.

With the use of instruments for measuring the number of aerosol particles (for example, a condensational particle counter, abbreviated as CPC by TSI), the eddy covariance (EC) method has been applied, and measurements of the aerosol particle number flux have become possible (Buzorius et al., 1998). The vertical turbulent flux of the aerosol particle number density  $F_p$  is denoted as a cross-covariance between the aerosol particle number concentration  $N'$  and the vertical wind speed  $w'$  (Ripamonti et al., 2013). To obtain vertical turbulent flux of the aerosol number density, the EC principle allows quantifying the number flux from fluctuation measurements. As a result, the vertical turbulent flux of the aerosol particle number density has been measured in many cities, such as in Toronto, Canada (Gordon et al., 2011), Stockholm, Sweden (Vogt et al., 2011b), Helsinki, Finland (Ripamonti et al., 2013), London, UK (Harrison et al., 2012), the Blodgett Forest Observatory in the United States (Farmer et al., 2011), and measurements of sea salt aerosol fluxes in northern Europe (Brooks et al., 2009; Sproson et al., 2013). These results have shown the

quantitative relationship among urban aerosol fluxes, urban vehicle emissions, and meteorological conditions (Jarvi et al., 2009) and have been used to determine transport characteristics of sea salt aerosol and provide further knowledge of aerosol properties (Nemitz et al., 2009). These measurements have been mainly collected in cities because of their anthropogenic contributions to aerosol emissions. These data can be used as routine model inputs. Direct eddy covariance measurements of aerosol exchanges in tropical forests, where primary biological aerosol particles represent a substantial fraction of the airborne particulate matter (Graham et al., 2003), were also performed by Ahlm et al. (Ahlm et al., 2010a; Ahlm et al., 2010b) and Whitehead et al. (Whitehead et al., 2010), potentially giving a proxy for microbial emissions in tropical ecosystems.

Although measurements of urban aerosol particle number density fluxes have been collected, the current eddy ~~correlation~~covariance method only provides fluxes for the aerosol particle number density at a point. We know that the underlying surface of a city is very complex, and thus the aerosol particle flux is not homogeneous in the horizontal. For a complex underlying surface such as a city, these point measurements are not very representative. Therefore, it is of great importance to design an aerosol flux measurement system with an accurate spatial representation.

The use of eddy ~~correlation~~covariance principles to measure sensible heat fluxes has been widely performed (Lee, 2004)(Lee, 2004). Current sensible heat fluxes can also be obtained using a large aperture scintillometer (LAS) based on the light propagation theory and similarity theory (Zeweldi et al., 2010)(Zeweldi et al., 2010). This configuration makes it ~~is~~ possible to achieve aerosol mass flux measurements using the light propagation theory and similarity theory. Recently, we measured the imaginary part of the atmospheric equivalent refractive index structure parameter based on the light propagation theory (Yuan et al., 2015)(Yuan et al., 2015). The results showed that the imaginary part of the atmospheric equivalent refractive index structure parameter is related to turbulent transport and the spatial distribution characteristics of aerosols. Experiments also showed that there is a strong correlation between the imaginary part of the atmospheric equivalent refractive index and the mass concentration of aerosol particles (Yuan et al., 2016)(Yuan et al., 2016). Thus, similar to the temperature structure parameter reflecting the sensible heat flux, the structural parameter of the imaginary part of the atmospheric equivalent refractive index can ~~reflect~~reveal the mass flux of aerosol particles. This paper attempts to measure the aerosol mass flux in the BTH area, especially during heavy aerosol pollution episodes.

To gain a deeper understanding of the interaction between atmospheric heavy pollution and weather in the BTH region, joint observations have been carried out in the BTH region since the winter of 2016 (Zhong et al., 2018b; Zhong et al., 2018a; Wang et al., 2018; Shen et al., 2018). The observations reveal the large-scale and mesoscale transport processes of aerosols between heavy pollution episodes (HPEs) in the BTH region in the winter of 2016. Most HPEs in the BTH region are due to horizontal transport and unfavourable meteorological conditions (Zhong et al., 2018a). However, during HPEs, no research has been conducted in the BTH area on quantifying the contribution of surface emissions to the concentration of pollutants. In this study, we focus on HPEs through field observations of aerosol transport based on the light propagation theory and surface similarity in the Beijing urban district and Gucheng suburban area.

Generally, based on the PM<sub>2.5</sub> daily mean mass concentration limit in the primary standard of China's national environmental quality standards (EPD, 2012), a pollution episode is referred to as the period during which the PM<sub>2.5</sub> concentration exceeds 80  $\mu\text{g m}^{-3}$  for 3 consecutive days between two clean periods, while a period when the PM<sub>2.5</sub> level is less than 35  $\mu\text{g m}^{-3}$  is defined as a clean

period. Pollution episodes with peak  $PM_{2.5}$  values of more than  $400 \mu g m^{-3}$  or less than  $300 \mu g m^{-3}$  are termed heavy-pollution episodes (HPEs) or light-pollution episodes (LPEs), respectively (Zhong et al., 2017b).

To gain a deeper understanding of the interaction between atmospheric heavy pollution and weather in the BTH region, joint observations have been carried out in the BTH region since the winter of 2016 (Zhong et al., 2018c; Zhong et al., 2018b; Wang et al., 2018; Shen et al., 2018). Based on meteorological causes of the increase or decrease in  $PM_{2.5}$  mass concentrations, an HPE in the BTH region can be divided into a transport stage (TS), an accumulative stage (AS) and a removal stage (RS). During the TS, the  $PM_{2.5}$  is dominated by relatively strong southerly winds, which carry polluted air masses from more populated southern industrial regions (Guo et al., 2014; Zhong et al., 2018a). Before rising processes during TSs, the urban  $PM_{2.5}$  mass concentration of Baoding, which is typically representative of pollution conditions in the south of Beijing, was much higher than Beijing; the winds in Beijing rapidly shifted from northerly to southerly. Then the rising in  $PM_{2.5}$  occurred, consistently with southerly slight or gentle breezes in the BL. The southerly air mass moves more than  $288 km d^{-1}$  below 500 m (estimated from the measured wind speed), which are fast enough to transport pollutants to Beijing. Such processes indicate southerly pollutant transport is primarily responsible for the rising, given the pollution transport pathway of the southwest wind belt determined by the unique geographic features of the North China Plain, with the Tai-hang Mountains and the Yan Mountains strengthening the southwest wind belt and leading the convergence of pollutant transport in Beijing (Su et al., 2004). During the ASs,  $PM_{2.5}$  increase is dominated by stable atmospheric stratification characteristic of southerly slight or calm winds, near-ground anomalous inversion, and moisture accumulation. When the vertical aerosols are accumulated to a certain degree, the dominant scattering aerosols will substantially back-scatter solar radiation, causing a reduction in the amount of solar radiation that reaches the surface, which creates a near-ground cooling effect through atmospheric circulation and vertical mixing (Zhong et al., 2018c). A feedback effect of further worsened meteorological conditions aggravates  $PM_{2.5}$  pollution (Zhong et al., 2017a). During the RSs, strong north-westerly winds whose velocity increases with height occur mostly. Strong northerly winds are from less populated north mountainous areas and carry unpolluted air masses to Beijing, which is favorable for pollution dispersion. The observations reveal the large-scale and mesoscale transport processes of aerosols between HPEs in the BTH region in the winter of 2016. However, during HPEs, no research has been conducted in the BTH area on quantifying the contribution of surface emissions to the concentration of pollutants. In this study, we focus on aerosol emission during HPEs through field observations of aerosol turbulent based on the light propagation theory and surface similarity in the Beijing urban district and Gucheng suburban area.

The second section of this paper introduces the theory of aerosol vertical ~~transport~~ turbulent flux measurements, the third section introduces the experiment, the fourth section gives the experimental results, and finally, the conclusion and discussion are presented in the fifth section.

## 2 Theory and methods

The ~~theory argument~~ for calculating the vertical flux of aerosol particles and the ~~theory approach~~ for calculating the friction velocity and characteristic temperature using the temperature and wind profiles is presented in the following subsections.

## 2.1 Calculation of the aerosol mass vertical flux

According to the micrometeorological principle (Stull, 1988), similar to the estimation method of the sensible heat flux, the aerosol flux  $F_a$  can be obtained as follows:

$$F_a = u_* M_* \quad (1)$$

where  $u_*$  is the friction velocity, which can be obtained from the temperature and wind speed profiles or directly from three-dimensional wind speed measurements; see Sec. 2.2. Prior experiments have shown that the motionspectral characteristics of aerosol particles in the atmosphere number concentration fluctuations approximate the motionspectral characteristics of general scalars molecular density fluctuations. (Martensson et al. 2006; Vogt et al. 2011b). Therefore, aerosol particles can be approximated as scalars for turbulent statistics, and characteristic parameters  $M_*$  similar to the scalars can be introduced, which can be regarded as the atmospheric aerosol mass concentration scale in the surface layer and deduced from surface layer similarity theory. This approximation is similar to the surface-layer temperature scale (Stull, 1988) as follows:

$$\frac{C_M^2 (z-d)^{2/3}}{M_*^2} = \eta(\xi) \quad (2)$$

where  $z$  is the measurement height,  $d$  is the zero-displacement height (Evans and De Bruin, 2011; Hartogensis et al., 2003),  $\xi = (z-d)/L$  is the nondimensional stability parameter,  $L$  is the Monin-Obukhov (M-OMO) length and defined as  $L = \frac{\bar{T} u_*^2}{\kappa g T_*}$  (Stull, 1988),  $\bar{T}$  is the average temperature,  $T_*$  is the surface-layer characteristic temperature,  $\kappa$  is the von Karman constant, which is 0.4, and  $g$  is acceleration due to gravity. The stability function ( $\eta(\xi)$ ) can be expressed as follows depending on the stability condition (DeBruin et al., 1995) (DeBruin et al., 1995):

$$\eta(\xi) = a_1 [1 - a_2 \xi]^{-2/3} \quad (3)$$

for unstable conditions ( $\xi < 0$ ), and the following:

$$\eta(\xi) = b_1 [1 + b_2 (\xi)^{e_1}] \quad (4)$$

for stable conditions ( $\xi \geq 0$ ) (Wyngaard et al., 1971).

In Eqs. (3) and (4),  $a_1$ ,  $a_2$ ,  $b_1$ ,  $b_2$  and  $e_1$  are constants, and different experiments have provided different values, although the differences between these results are small. Here, we take the

域代码已更改



parameters  $a_1=4.9$ ,  $a_2=9$ ,  $b_1=5$ , and  $b_2=0$  (DeBruin et al., 1995).

In Eqs. (3) and (4),  $a_1$ ,  $a_2$ ,  $b_1$ ,  $b_2$  and  $e_1$  are constants, and different experiments have provided different values, although the differences between these results are small. It is assumed that the aerosol mass concentration fluctuation characteristics are the same as the temperature fluctuation characteristics and the same similarity law of Eq. (2) is satisfied. Therefore, based on the

experimental data, the values of  $\sqrt{\frac{C_M^2(z-d)^{2/3}}{\eta(\zeta)}}$  and  $T_*$  are calculated using various schemes.

After comparing the differences between the two, the scheme of DeBruin et al (DeBruin et al., 1995) with  $a_1=4.9$ ,  $a_2=9$ ,  $b_1=5$ , and  $b_2=0$  is taken with a minimum difference.

$C_M^2$  in Eq. (2) is the aerosol mass concentration structure parameter. We assume that the aerosol particles in the atmosphere follow the movement of the air and satisfy the turbulent motion law. Previous studies have shown that the particle concentration fluctuation spectra follow a ‘-5/3’ power law under unstable stratification conditions (Martensson et al., 2006; Vogt et al., 2011b), and the velocity-concentration co-spectra follows a ‘-4/3’ power law (Martensson et al., 2006; Vogt et al., 2011a; Kaimal et al., 1972)(Martensson et al., 2006; Vogt et al., 2011a; Kaimal et al., 1972).

Thus, the distributionsimilarity of small particles can be considered as a conservative passive quantity analogous to theatmospheric aerosols and temperature can be assumed for the purpose.

Then, at a separation ( $r$ ) of the order in the inertial subrange in a locally isotropic field, the aerosol mass concentration (denoted as  $M_a$ ) structure function ( $D_M(r)$ ) follows a “2/3 law” (Wyngaard, 2010)(Wyngaard, 2010) and can be expressed as  $\overline{D_M(r)} = \overline{[M_a(x) - M_a(x+r)]^2} = C_M^2 r^{2/3}$ , where  $x$  is the position vector,  $r$  is the separation vector, and the overbar indicates the spatial average.

The following describes the method to deduce the aerosol mass concentration structure parameter  $C_M^2$ .

We assume that the aerosol particles are continuously dispersed in the air. Although the aerosol particles are dispersed in the air, the macroscopic behavior of the gas-particle two-phase mixture is the same as if it is perfectly continuous in structure and physical quantities, such as the mass and refractive index associated with the matter contained within a given small volume, which will be regarded as being spread continuously over that volume. The aerosol particles and gases in the atmosphere can be considered as an equivalent medium, and an atmospheric equivalent refractive index (AERI)  $n_{equ}$  is introduced that contains the real part  $n_{re}$  and the imaginary part  $n_{im}$  of the equivalent refractive index. Thus,  $n_{equ}=n_{re}+i \bullet n_{im}$ . For visible light, the attenuation of light by gases

带格式的：字体颜色：自动设置

带格式的：字体颜色：自动设置

in the atmosphere is very weak; the cause of the attenuation is the absorption and scattering due to aerosol particles. Therefore, the real part of the equivalent medium of aerosol particles and gases is determined by the gas composition of the air. The fluctuation of the real part is mainly determined by temperature fluctuations; the imaginary part is determined by the aerosol particles, and the fluctuation of the imaginary part is determined by fluctuations in the aerosol concentration.

For visible light, there is a strongerobust linear relationship between the variation of the real part of the AERI and the variation of the atmospheric temperature, i.e.,  $R_{TN} = \frac{\delta T}{\delta n_{Re}}$  namely,

$R_{TN} = \frac{\delta T}{\delta n_{Re}}$ ; thus, we have the following:

$$R_{TN} = -1.29 \times 10^4 \times \left(1 + \frac{7.52 \times 10^{-3}}{\lambda^2}\right)^{-1} \frac{\bar{T}^2}{\bar{P}} \quad (5)$$

which is based on the relationship between the real part of the AERI ( $n_{Re}$ ) and atmospheric temperature (~~Tatarskii, 1961~~)(Tatarskii, 1961). Because the wavelength is deterministic, the ratio  $R_{TN}$  can be obtained by measuring the atmospheric temperature. The imaginary part of the AERI ( $n_{Im}$ ) has a close correspondence with the extinction coefficient of the equivalent medium, and the extinction coefficient is inversely proportional to the visibility. The light wavelength is selected as 0.620  $\mu m$ . This wavelength is only weakly absorbed by  $O_3$ ; therefore, the observed absorption is primarily due to aerosol (Brion et al., 1998; Lou et al., 2014; Nebuloni, 2005). Higher concentrations of aerosols in the atmosphere are related to lower visibility and vice versa; thus, the relationship between the imaginary part of the AERI and the atmospheric aerosol mass concentration can be established. The ratio of the atmospheric aerosol mass concentration to the imaginary part of the AERI  $R_{MN}$  can be defined as follows:

$$R_{MN} = \frac{M_a}{n_{Im}}. \quad (6)$$

Theoretical analysis has revealed that  $R_{MN}$  is associated with the aerosol particle size distribution, mass density of the aerosol particles, and the aerosol particle refractive index. Because of the relatively small variations in particle size and aerosol refractive index (~~Dubovik et al., 2002~~)(Dubovik et al., 2002),  $R_{MN}$  can be treated as a constant for surface-layer aerosols at a given location. Of course,  $R_{MN}$  can be obtained by simultaneously measuring  $M_a$  and the imaginary part of the AERI, so that real-time  $R_{MN}$  can be obtained.  $M_a$  approximates the  $PM_{10}$  value. The variable  $n_{Im}$  can be calculated as follows (~~Yuan et al., 2016~~)(Yuan et al., 2016):

带格式的: 段落间距段后: 0 磅

$$n_m = \frac{0.55e-6}{4\pi} \cdot \frac{3.912}{L_v} \quad (7)$$

where the unit of visibility ( $L_v$ ) is m.

According to Eqs. (5) and (6), we have the following:

$$C_T^2 = R_{TN}^2 C_{n,Re}^2 \quad (8)$$

$$C_M^2 = R_{MN}^2 C_{n,Im}^2 \quad (9)$$

Thus, the temperature structure parameter  $C_T^2$  and the aerosol mass concentration fluctuation structure parameter  $C_M^2$  are converted into the measurement of the real and imaginary ~~structure~~structural parameters of the AERI, namely,  $C_{n,Re}^2$  and  $C_{n,Im}^2$  respectively.

The measurement of relevant parameters is performed based on the light propagation theory. When light is transmitted in an equivalent medium, the AERI fluctuation will cause light fluctuations in light intensity. ~~Theoretical~~When the attenuation caused by scattering and experimental results have shown that the absorption along the propagation path is very weak, light intensity fluctuation can be decomposed into high-frequency and low-frequency fluctuations. The high-frequency fluctuations are determined by fluctuations depends on the fluctuation of the real part of the AERI, and the low-frequency fluctuations are determined along the propagation path. When the attenuation caused by fluctuations scattering and absorption along the propagation path is relatively strong, the light intensity fluctuation is also related to the fluctuation of the imaginary part of the AERI along the propagation path. With the spectral analysis method, the LAS light intensity fluctuations can be separated into the contributions of the real and imaginary parts of the AERI. The contribution of the real part of the AERI corresponds to the high frequencies, whereas the contribution of the imaginary part of the AERI corresponds to the low frequencies, suggesting that the variances resulting from the real and imaginary parts are independent. Therefore, the light intensity variances induced by the real and imaginary parts can be detected separately at high frequencies and low frequencies from the LAS measurements (Yuan et al., 2015). Thus, the real and imaginary structure parameters of the ~~equivalent refractive index~~AERI can be calculated by our developed LAS.

So far, we have completed the estimation of the aerosol mass ~~transport~~turbulent flux.

According to the previous derivation and analysis, there are two calculation schemes for

带格式的：非上标/ 下标

determining the aerosol mass flux as follows:

$$F_{a1} = \left( \frac{C_{n,\text{Im}}^2}{C_{n,\text{Re}}^2} \right)^{1/2} \frac{R_{MN}}{R_{TN}} u_* |T_*| \quad (10)$$

$$F_{a2} = u_* \sqrt{\frac{C_M^2 z^{2/3}}{\eta(\xi)}} = u_* R_{MN} \sqrt{\frac{C_{n,\text{Im}}^2 z^{2/3}}{\eta(\xi)}} \quad F_{a2} = u_* \sqrt{\frac{C_M^2 (z-d)^{2/3}}{\eta(\xi)}} = u_* R_{MN} \sqrt{\frac{C_{n,\text{Im}}^2 (z-d)^{2/3}}{\eta(\xi)}} \quad (11)$$

When the free convection approximation ( $-\xi \gg 1$ ) is assumed, based on the definition of the M-O length, and the similarity theory (Wyngaard et al., 1971)(Wyngaard et al., 1971), the following can be obtained:

$$F_{a3} = a \left( \frac{g}{T} \right)^{1/2} R_{TN}^{1/2} (C_{n,\text{Re}}^2)^{1/4} R_{MN} (C_{n,\text{Im}}^2)^{1/2} (z-d) \quad (12)$$

where the coefficient  $a = a_1^{-3/4} a_2^{1/2} K^{1/2}$  can be taken as 0.567 (DeBruin et al., 1995; Lagouarde et al., 2006)(DeBruin et al., 1995; Lagouarde et al., 2006). Eqs. (10)-(12) are the theoretical basis for the aerosol mass flux measurements.

According to Eqs. (10)-(12), the vertical ~~transport~~turbulent flux of aerosol particles is related to the strength of turbulent fluctuations of temperature and aerosol mass concentration fluctuations.

Based on the discussion above, the LAS technique is capable to determine the magnitude of the flux but not the sign. In general, the aerosols are very heterogeneous in space and the measured fluxes show typically large variation in magnitude including the sign. Over the polluted areas, which behave as the source, the emissions presumable overwhelmingly exceed the deposition sinks (Ripamonti et al., 2013). Therefore, a rough quantification of the deposition sink would allow concluding that the sink term is negligible and the flux quantified by LAS can be assumed to represent the upward fluxes.

## 2.2 Calculation of the friction velocity and surface-layer characteristic temperature

To calculate the aerosol vertical ~~transport~~turbulent flux, according to Eq. (10), the values of the friction velocity  $u_*$  and the characteristic temperature  $T_*$  are required. These can be obtained via wind speed and temperature profile data. From the near-surface similarity theory, the temperature and wind speed data measured at two heights of  $z_1$  and  $z_2$  can be used in the expressions of the friction velocity  $u_*$  and the characteristic temperature  $T_*$  (Stull, 1988)(Stull, 1988) as follows:

$$u_* = \frac{\kappa[U(z_2) - U(z_1)]}{\ln \frac{z_2}{z_1} - \Psi_b(\xi_2) + \Psi_b(\xi_1)} \quad (13)$$

$$T_* = \frac{\kappa[T(z_2) - T(z_1)]}{0.74[\ln \frac{z_2}{z_1} - \Psi_r(\xi_2) + \Psi_r(\xi_1)]} \quad (14)$$

where  $U(z_1)$  and  $U(z_2)$  are the measured velocities at heights  $z_1$  and  $z_2$ , respectively,  $T(z_1)$  and  $T(z_2)$

are the measured temperatures at heights  $z_1$  and  $z_2$ , respectively,  $\zeta_1$  and  $\zeta_2$  are the stabilities at heights  $z_1$  and  $z_2$ , respectively, and  $\Psi_U$  and  $\Psi_T$  are the correction terms for the velocity and temperature profiles under the condition of stability  $L$ . Under unstable conditions (Stull, 1988)(Stull, 1988), we have the following:

$$\Psi_U(\xi) = \ln\left[\left(\frac{1+x^2}{2}\right)\left(\frac{1+x}{2}\right)^2\right] - 2\arctan(x) + \frac{\pi}{2}, \quad x = (1-15\xi)^{1/4} \quad (15)$$

$$\Psi_T(\xi) = \ln\left[\left(\frac{1+y}{2}\right)^2\right], \quad y = (1-9\xi)^{1/2} \quad (16)$$

Under stable conditions (Cheng and Brutsaert, 2005), we have the following:

$$\Psi_U(\xi) = -a \ln[\xi + (1 + \xi^b)^{1/b}], \quad a=6.1, b=2.5. \quad (17)$$

$$\Psi_T(\xi) = -c \ln[\xi + (1 + \xi^d)^{1/d}], \quad c=5.3, d=1.1. \quad (18)$$

Based on Eqs. (13)-(18), the friction velocity  $u_*$  and characteristic temperature  $T_*$  can be determined.

### 3 Measurements and data processing

#### 3.1 Introduction of Experiments

Observations were collected at two locations (two rectangles in Fig. 1a) from December 2016 to March 2017: a rural site in Gucheng (GC site), Hebei Province and an urban site at the Chinese Academy of Meteorological Sciences (CAMS site) in Beijing. The distance between the two locations is approximately 100 km. According to the theoretical methods defined in the preceding section, to estimate the aerosol transport turbulent flux, the ratio of the aerosol mass to the imaginary part of the AERI, the ratio of the temperature to the real part of the AERI, the real and imaginary parts of the atmospheric equivalent refractive index structure parameter (AERISP,  $C_{n,Re}^2$  and  $C_{n,Im}^2$ ), the friction speed, and the characteristic temperature must all be obtained. If the free convection condition is satisfied, fewer parameters are required, including the real and imaginary parts of the AERISP, the ratio of the aerosol mass to the imaginary part of the AERI, the ratio of the temperature to the real part of the AERI, and the atmospheric temperature.

Two sets of LASs developed by our research group were installed at the top of the building of the Beijing Institute Chinese Academy of Meteorological Sciences (point A in Fig. 1b) and at the top of a two-story building in the farm of the Central Meteorological Bureau of Gucheng Town, Baoding City (point D in Fig. 1c). The light intensity sampling frequency of the receiving end was 500 Hz, and a file was recorded every 20 minutes. Then, the real and imaginary parts of the AERISP were calculated.

In the CAMS site, the transmitter end of the LAS was placed on the roof of a building on the east side of the Institute Chinese Academy of Meteorological Sciences, and the receiver end was placed at the top of the Chinese Academy of Meteorological Sciences. The propagation path was along an east-west direction. The distance between the two ends was 550 metresmeters as shown in Fig. 1d. The light beam passed over urban buildings, residential areas and urban roads. The beam height was 43 metresmeters. The average height of the building below the beam was 24 metresmeters; thus, the zero-displacement was 18 metresmeters ( $24 * 0.67 = 18$ ) (Leclerc and Foken, 2014)(Leclerc and

域代码已更改

带格式的：字体：倾斜

带格式的：缩进：首行缩进： 0 字符

Foken, 2014), and the effective height of the beam was 25 metres. At the Beijing observation point, the temperature and wind speed of the near-surface atmosphere were conventional meteorological parameters are measured simultaneously, and on the same roof, 20 meters away from the receiving end and in the northwest direction of the receiving end. The measurement heights were 1.5 m and 10 m, respectively, above the roof for air temperature and wind speed. To calculate the aerosol flux, it is necessary to obtain the ratio of the aerosol mass to the imaginary part of AERI and to measure the aerosol mass concentration and visibility. In Haidian District, there is a site to measure the visibility of the near-surface layer (point B in Fig. 1b), and the PM<sub>10</sub> mass concentration measurements were collected at Guanyuan Station (see point C in Fig. 1B). The sampling interval for the visibility and PM<sub>10</sub> mass concentration measurements was 1 h. The measurement height of points B and C in Fig. 1b was approximately 20 metres. The ratio of the aerosol mass PM<sub>10</sub> to the imaginary part of the AERI was calculated based on the data. The measurements were collected at the CAMS site from 15 January 15, 2017 to 20 March 20, 2017.

In the GC site (point D in Fig. 1c, namely, the LAS position) in Gucheng, Baoding, Hebei, the transmitter of the LAS was placed on the roof of a two-story building with a height of 8 m, and the receiving end was located in a room in a three-story building on the west side of National Highway 107 at the same height as the transmitting end. The distance between the transmitting end and the receiving end was 1670 metres. The terrain between the transmitting end and the receiving end was flat, with farmland, a national road and sporadic trees below the beam, as seen in Fig. 1e. Near the light beam, there was a 30-metre-high meteorological observation tower, in which the temperature, relative humidity (RH), and wind speed were measured at five levels (1 m, 3 m, 8 m, 18 m, and 28 m). The friction speed and characteristic temperature were calculated according to the temperature wind speed profile. Visibility observations were made in Xushui District near the LAS position (see point E in Fig. 1c). The PM<sub>10</sub> mass concentration was measured in Beishi District (see point F in Fig. 1c). From Fig. 1c, the three observation points (points D, E and F in Fig. 1c) formed a nearly straight line and were distributed in a northeast-southwest direction. During the experimental observation period, a northeast-southwest wind prevailed; thus, the Xushui District visibility data and Beishi District PM<sub>10</sub> data can approximate the situation of the scintillometer position. The measurements were collected at the GC site from 17 November 17, 2016 to 30 March 30, 2017.

### 3.2 Data quality control

There are two types of variables, e.g., namely mean variables and fluctuation variables. Mean variables include temperature, wind speed, wind direction, PM<sub>10</sub>, and visibility for averages of 30 minutes or 60 minutes. Data quality control for the mean variables was conducted by comparing the measured data at different heights or from personal experience at different stations. Same variables between different heights and different locations having the same trend are considered high quality. All the measured mean data were determined to be adequate. Fluctuation variables include the high-frequency intensity fluctuation data measured by the LAS, the real and imaginary parts of the AERISP, and the calculated aerosol flux. Quality control mainly includes consists of the elimination of spike and supplementing missing data.

Peaks in the light intensity fluctuation data appear because the received signal quickly increases when the light signal is blocked, such as due to birds along the transmission path. This situation is

The data processing program automatically determines this situation. When this happens, the current 20-minute period is rejected. For the real and imaginary parts of the AERISP and the aerosol flux data, (a) 3 times the standard deviation (SD) of the anomaly and (b) 3 times the SD of the adjacent difference between adjacent moments (AMD) were determined. The method for judging 3 times the SD of the anomaly was applied to obtain a trend of two-hour averages, namely, 6-point moving averages, is first obtained. Then, the difference between the measured value and the trend at each moment was calculated, and the mean and SD of the difference were also calculated. The data with differences from the trend exceeding 3 times the SD were considered as spikes. The method for judging the difference of 3 times the SD of the adjacent differences AMD was to first to calculate the difference between adjacent observations AMD and then calculate the mean and SD of the difference AMDs. Any data whose adjacent difference AMD deviated from the mean of the adjacent difference AMD by more than 3 the SD of the AMD was considered an error. Less than 5% of the data were considered found to contain spikes or errors.

The data determined to be errors were supplemented by with the average of the nearby observations. Of course, if data were missing over a long period, the missing gap could not be filled. For this situation, further supplementation was not considered.

Other errors in the measurements using a LAS due to specific reasons (Moene et al., 2009)(Moene et al., 2009); for example, the impact of the uncertainty in the exact shape of the turbulence spectrum with von Karman's scheme and the intermittent variations in the characteristics of that spectrum on the LAS signal were not considered in this study.

## 4 Results

First, the visibility and PM<sub>10</sub> aerosol mass concentration results at the CAMS site and the GC site are given and compared. Then, the characteristics of aerosol transport in typical weather conditions at the CAMS site and the GC site are discussed. Finally, the aerosol flux characteristics under heavy pollution weather conditions are analysed during the HPEs are analyzed.

### 4.1 Relationship between $n_{im}$ and PM<sub>10</sub>

To obtain the ratio of the atmospheric aerosol mass concentration to the imaginary part of the AERI ( $n_{im}$ )  $R_{MN}$ , PM<sub>10</sub> and visibility were measured.

The maximum PM<sub>10</sub> concentration in the Baoding area appeared at 1:00 on January 28, 2017 (up to 1071  $\mu\text{g m}^{-3}$ ), and the maximum PM<sub>10</sub> concentration in the Beijing area appeared at 2:00 on January 28, 2017 (up to 917  $\mu\text{g m}^{-3}$ ). This heavy pollution event swept through Beijing and the surrounding areas, reaching a maximum at almost the same time. The visibility at the corresponding time was less than 500 metres. The imaginary part of the AERI can be calculated from the visibility (Yuan et al., 2016) meters. The imaginary part of the AERI can be calculated from the visibility according to Eq. (7). Fig. 2a shows a scatter diagram of the imaginary parts of the AERI and PM<sub>10</sub> data measured in the Beijing area; there is a strong correlation between the AERI and aerosol particle mass concentration, with a linear correlation coefficient of 0.96. The fitted linear in Fig. 2a has a slope of 3845  $\text{kg m kg m}^{-3}$ . Therefore,  $R_{MN}$  was taken as 3845  $\text{kg m kg m}^{-3}$  for the Beijing area to estimate the aerosol vertical transportation turbulent flux. Similarly, Fig. 2b shows the results for the Baoding area, and  $R_{MN}$  was set to 3711  $\text{kg m kg m}^{-3}$  for the Baoding area to estimate the aerosol

vertical ~~transportation~~turbulent flux. The two ratio coefficients are relatively close. Figs. 2a and 2b also show that in the case of light pollution, Beijing's  $R_{MN}$  is slightly larger.

Furthermore, Figs. 2a and 2b show that although there is a ~~largesignificant~~ scattering between  $PM_{10}$  and  $n_{IM}$  that may be attributed to a ~~largesignificant~~ separation between the two measurement locations for visibility and  $PM_{10}$ , there is a strong linear correlation between the imaginary part of the AERI and  $PM_{10}$ . The imaginary part of the AERI has a slightly stronger ~~correlationrelationship~~ with the  $PM_{10}$  data obtained in the Baoding area than in the Beijing area.

$R_{MN}$  should be obtained by simultaneously measuring  $Ma$  and the imaginary part of the AERI at the same location with the LAS, so that real-time RMN can be obtained. For GC site and CAMS site, measuring positions of  $PM_{10}$  and visibility are a little far from LAS measurement. So a constant ratio  $R_{MN}$  is more representative than a simultaneous value.

The following provides the results of the aerosol ~~transportturbulent~~ flux under typical weather conditions in Beijing and Baoding for the period from 10 March 10, 2017 to 17 March 17, 2017.

#### 4.2 Characteristics of aerosol flux in the Beijing region

To ~~analyseanalyze~~ the aerosol ~~transportturbulent~~ flux characteristics, we present the time series of the conventional meteorological parameters. ~~The measurement site is the Beijing Meteorological Observatory, which is 20 metres above the ground.~~ The time series of temperature, RH, wind speed, wind direction,  $PM_{10}$ ,  $C_{n,Re}^2$ ,  $C_{n,Im}^2$  and aerosol flux are shown in Figs. 3a-3h, respectively. The temperature has ~~an-obviousa distinct~~ diurnal variation, indicating that this period had primarily sunny weather. The RH from 10 March 10, 2017 to 17 March 17, 2017, was less than 60%, and the RH for most of the ~~time~~ period was less than 30%. The wind speed was low; only during the period from March 11 to March 14 was the wind strong. At 6:00 on March 12, the maximum wind speed was  $4.2 \text{ m s}^{-1}$ . ~~At that time, there was no dominant wind direction. At that time, the wind direction has diurnal variation characteristics, which are related to the sea-land breeze, valley wind and urban heat island circulation which may exist under the control of weak weather system (Li et al., 2019).~~ Moreover, two light pollution events occurred ~~(MEP, 2012)(MEP, 2012)~~ on March 11 and March 16, with  $PM_{10}$  concentrations approaching  $200 \mu\text{g m}^{-3}$ . From the data of  $C_{n,Re}^2$  and  $C_{n,Im}^2$  in Figs. 3f and 3g, the real part of the AERISP  $C_{n,Re}^2$  has obvious diurnal variations, i.e., smaller in the morning and at night and larger at noon. The imaginary part of the AERISP  $C_{n,Im}^2$  had no ~~obviousdistinct~~ diurnal variation. According to Fig. 3g, there are some peak values, i.e., some sudden increases and decreases, which may be related to sudden changes in wind direction, as shown in Fig. 3d.

Aerosol fluxes in Beijing are calculated using the assumption of free convection. The LAS at the CAMS site was located in the roughness layer, so the local similarity theory should in principle applied to flux calculation. Because there was no measurement of wind speed and temperature profiles near the LAS measurement location, the friction velocity and characteristic temperature could not be calculated. ~~Because the height of the LAS instrument at the CAMS site was 43 m. We (Yuan et al, 2015) conducted a test experiment for aerosol vertical flux in Hefei, China, using free convection assumptions and local similarity theories to calculate aerosol fluxes. Comparison of the calculation results of the two methods shows that very unstable condition accounts for about 62 % of the time, and the relative difference is about 5%. Under weak unstable and stable condition, the relative error is about 15%. Although the relative error is a little large under weak unstable stable stratification conditions, the absolute difference in flux is still small.~~



There is a weather tower in the north of Beijing. The weather tower is 6.1km far from the CAMS site. The meteorological observation data from the weather tower show that the Monin-Oubhov similarity theory has a significant error under stable condition, while the Monin-Oubhov similarity theory is still basically applicable in the case of unstable stratification (Liu et al. 2009). In the roughness sub-layers of other cities, under the condition of unstable stratification, the local similarity theory is similar to MOST (Zou et al. 2018, 2019). Because the height of the LAS instrument at the CAMS site was 43 m, during most of the time the conditions assumed for free convection were easily satisfied. During the day, the surface layer is usually unstable. At night, for the city, even if there is an inversion at a higher altitude, due to the existence of the urban heat island, the surface layer is often weakly unstable. The stable stratification situation is rare (Li et al., 2007)(Li et al., 2007). Therefore, aerosol fluxes in Beijing are calculated using Eq. (12) based on the assumption of free convection.

From the aerosol flux time series given in Fig. 3h, the aerosol flux is large at noon and small in the morning and at night, which is mainly because of the strong convection at noon. However, large aerosol fluxes also occurred on the nights of March 11 and March 12, which were related to high wind speeds. The mean aerosol flux measured at this observation point during this period was  $0.0039 \text{ mg m}^{-2} \text{ s}^{-1}$ .

#### 4.3 Characteristics of aerosol flux at the GC site

Similarly, Figs. 4a-4d provide the time series of temperature, RH, wind speed and wind direction at 3 metres and 18 metres for the GC site, and Figs. 4e-4h show the  $\text{PM}_{10}$ ,  $C_n$ ,  $R_e^2$ ,  $C_n$ ,  $l_m^2$  and aerosol flux curves over time. According to Fig. 4a, the temperatures at both heights show obvious distinct diurnal variations. The daytime is characterized by unstable stratification, and at night, stable stratification prevails. Moreover, in the morning and evening, there is a transition period between the stable and unstable stratification. Here,  $u^*$ ,  $T^*$  and MO length  $L$  were calculated from the wind speed and temperature measured at 3 m and 18 m on a meteorological tower. Fig. 4b shows a plot of the two levels of RH over time, again with obvious apparent diurnal variations. The RH of the GC site was lower at the CAMS site. Figs. 4c and 4d provide the time series of wind speeds and wind directions at two levels. At 6:00 on March 12, the wind speed was relatively high, and the maximum at 18 metres was  $6.5 \text{ m s}^{-1}$ . At the same time, the maximum wind speed was reached in the Beijing area, although the speed was lower in Beijing. The overall trend of wind direction at the GC site was more consistent with the results of the CAMS site.

Figure 4e shows the  $\text{PM}_{10}$  trend of over time. There were two light pollution events on March 11 and March 16. The overall trend is the same as in Fig. 3(e) except that there is a slight difference. Figs. 4f and 4g show the time series of the imaginary and real parts of the AERISP for the GC site. The real part of the AERISP is large at noon, and the optical turbulence is strong. The real part of the AERISP is small during the morning and evening, and the corresponding turbulence is weak. The imaginary part of the AERISP given in Fig. 4g does not show an obvious apparent diurnal variation, and there may be some sharp peaks.

Figure 4h shows the aerosol mass vertical flux changes over time. The aerosol flux has a significant diurnal variation characteristic associated with turbulent transport near the surface. The mean aerosol flux measured at the GC site during this period was  $0.0016 \text{ mg m}^{-2} \text{ s}^{-1}$ . This value is much smaller than the results for the CAMS site. Human activities contribute to increased

water vapor releases in urban areas compared to rural areas, as observed by [Dou et al. \(2014\)](#) ([Dou et al., 2014](#)), and especially for the night-time SBL in winter. During our observation period, the RH of the city was lower than the rural area. However, human activities cause more aerosol particles in urban areas than in rural areas.

#### 4.4 Aerosol flux during heavy pollution periods

In the winter of 2016, there were several heavy pollution events. Generally, based on the  $PM_{2.5}$  daily mean mass concentration limit in the primary standard of China's national environmental quality standards (EPD, 2012), a pollution episode is referred to as the period during which the  $PM_{2.5}$  concentration exceeds  $80 \mu g m^{-3}$  for 3 consecutive days between two clean periods, while a period when the  $PM_{2.5}$  level is less than  $35 \mu g m^{-3}$  is defined as a clean period. Pollution episodes with peak  $PM_{2.5}$  values of more than  $400 \mu g m^{-3}$  or less than  $300 \mu g m^{-3}$  are termed heavy pollution episodes (HPEs) or light pollution episodes (LPEs), respectively (Zhong et al., 2017).

A heavy pollution event began on December 1, 2016 and ended on January 10, 2017. HPEs. A heavy pollution event began on 1 December 2016 and ended on 10 January 2017. Relevant observational experiments were performed in the Beijing and Baoding areas, including observations of meteorological parameters and aerosol parameters, to understand the causes of the heavy pollution. The observations show that the beginning of the HPE was characterized by pollutant transport under southerly conditions, i.e., the formation of heavy pollution was mainly caused by the pollutants transported from southern Beijing, which we call the transport stage (TS). Usually, after the TS stage, the explosive growth of  $PM_{10}$  and the rapid accumulation of pollutants occur, which is called the accumulative stage (AS). During the other period within the HPEs, aerosol particles are usually removed from the atmosphere, which is called the removal stage (RS). During heavy pollution events, there is a lower boundary layer depth, low wind speeds and high RH, and the  $PM_{10}$  concentration increases rapidly and reaches a very high value (Zhong et al., 2017). There

According to the definition of HPEs and classification, there were 7 TS stages in the 2016 winter heavy pollution event, and the AS stage appeared immediately after 4 TS stages. These included 00:00 on December 1 to 03:20 on December 4, 18:40 on December 15 to 00:00 on December 22, 00:00 on December 29 to January 2, and 00:00 and 8:40 on January 2 to 00:00 on January 5.

During this period, we used a LAS to conduct an observational study of the aerosol-vertical aerosol flux in the GC site, which was from 00:00 on December 1, 2016, to 00:00 on December 22, 2016. No corresponding observations were made at the Beijing site during this period. Here, we first discuss the observation results of the GC site, Baoding City, as shown in Fig. 5. Fig. 5a shows the time series of the aerosol vertical transport turbulent flux. Figs. 5b-5g show indicate the time series for the real and imaginary parts of the AERISP, the temperature and RH at 18 metres meters, and the wind speed and direction. Purple curves indicate the TS stages, red curves indicates show the AS stages, and grey curves indicates show the RS stages.

According to Fig. 5a, in the TS stages and the RS stages, the aerosol flux exhibited diurnal variations, while the AS stage did not show a diurnal variation. There were some peaks in the TS stage. The average aerosol flux of the TS stages was  $0.00065 mg m^{-2} s^{-1}$ , the average value of the AS stages was  $0.00025 mg m^{-2} s^{-1}$ , and the average value of the RS stages was  $0.00063 mg m^{-2} s^{-1}$ . The aerosol transport turbulent fluxes in the TS and RS stages were similar, while

the aerosol ~~transport~~<sup>turbulent</sup> flux in the AS stage was much smaller than the TS and RS stages.

According to Fig. 5b-5c, the imaginary structure parameters and the real structure parameters of the refractive index in the TS and RS stages exhibited diurnal variations, while the AS stage did not exhibit a diurnal variation. Fig. 5d shows that except for the second AS event (22:00 on ~~19~~ December ~~19~~-2016 to 00:00, ~~22~~ December-~~22~~, 2016), the temperature showed a diurnal variation. During the AS stage, the RH (see Fig. 5e) was close to 100%, while the RH during the TS and RS stages ~~was were~~ lower. Moreover, Fig. 5f shows that during this time, the wind speed was relatively weak, although the wind speed was slightly stronger on December 5. As shown in Fig. 5g, during the TS and AS stages, southerly winds prevailed, while during the RS period, northerly winds prevailed. The high wind speed and convection in the TS and RS stages contributed to the upward transport of aerosol particles, whereas the low wind speed and stable stratification in the AS stage were not conducive to the upward transport of aerosol particles.

During the heavy pollution period from ~~1~~ December ~~1~~-2016 to ~~10~~ January-~~10~~, 2017, we did not conduct surface aerosol flux observations at the CAMS site. From January 25 to January 31, the pollution in the Beijing area also reached the level of heavy pollution. During this ~~heavy pollution period~~<sup>HPE</sup>, a measurement of surface aerosol fluxes at the CAMS site was conducted. Figure 6 shows the results of the meteorological and pollutant observations for ~~6~~<sup>six</sup> days from 00:00 on January 25, 2017 to 00:00 on January 31, 2017. According to Fig. 6, northerly winds prevailed after ~~12:00 noon~~ on January 26, when the concentration of PM<sub>10</sub> dropped rapidly from 254  $\mu\text{g m}^{-3}$  at 12:00 to 5  $\mu\text{g m}^{-3}$  at 15:00. During the period 12:00-24:00 on January 26, the average wind speed was 2.6  $\text{ms}^{-1}$ . On January 27, southerly winds prevailed, the average wind speed was only 0.8  $\text{ms}^{-1}$ , and the aerosol concentration (PM<sub>10</sub>) increased slowly; the increase began at 6:30 before ~~increasing~~<sup>growing</sup> rapidly at 17:50, reaching more than 300  $\mu\text{g m}^{-3}$  at 23:00 and 917  $\mu\text{g m}^{-3}$  at 2:00 am on January 28, which was the maximum aerosol concentration over the 6 day period. Then, the aerosol concentration decreased gradually. The average wind speed on January 27 was 0.6  $\text{ms}^{-1}$ , southerly winds prevailed, and the mean PM<sub>10</sub> concentration was 440  $\mu\text{g m}^{-3}$ , which constitutes a ~~serious~~<sup>severe</sup> pollution level. The average PM<sub>10</sub> concentration during the period from 00:00 on January 25 to 00:00 on January 31 was 170  $\mu\text{g m}^{-3}$ .

According to the previous characteristics for the TS and AS stages, a period of southerly winds can be determined as the TS stage. Thus, January 27 can be designated as the TS stage, January 28 can be determined as the AS stage, and January 29 can be determined as the RS stage. During Beijing's heavy pollution event in January 2017 (20170125-20170131), the mean aerosol vertical flux in the TS stage was 0.0024 ~~mg m<sup>-2</sup> s<sup>-1</sup>~~<sup>mg m<sup>-2</sup> s<sup>-1</sup></sup>, the average value during the AS stage was 0.00087 ~~mg m<sup>-2</sup> s<sup>-1</sup>~~<sup>mg m<sup>-2</sup> s<sup>-1</sup></sup> and the RS stage was 0.0049 ~~mg m<sup>-2</sup> s<sup>-1</sup>~~<sup>mg m<sup>-2</sup> s<sup>-1</sup></sup>. The overall average value was 0.0032  $\text{mg m}^{-2} \text{s}^{-1}$ .

Even during heavy pollution events, the RH in Beijing was lower than in the outer suburbs. According to Fig. 6e, the RH exceeded 60% in the period from 3:00 to 6:00 on January 26, where the maximum value was 63%, and the RH was less than 60% in the remaining periods. In urban areas, when the RH is low, heavy pollution incidents can occur. In Beijing, during the AS stage, the vertical flux of aerosol was less than during the TS and RS stages.

## 5 Discussions and conclusions

During the winter of 2016 and the spring of 2017, HPEs ~~occurred~~<sup>occurred</sup> frequently in the BTH area.

This study investigated the aerosol vertical mass flux and compared its magnitude during different stages of HPEs, including RSs, TSs, and ASs, in two representative urban and rural sites, including the CAMS site in Beijing and the GC site in Hebei Province. Based on the light propagation theory and surface-layer similarity theory, the aerosol vertical mass flux was obtained by combining LAS observations, surface PM<sub>2.5</sub> and PM<sub>10</sub> mass concentrations, and meteorological observations, including air temperature and RH. We found that under ~~favourable~~favorable meteorological conditions for pollution dispersion, i.e., from 10 March 10, 2017 to 17 March 17, 2017, the vertical aerosol mass flux exhibited striking diurnal variations, with the mass fluxes reaching peak values at noon and lowering in the morning and evening. During the HPEs from 25 January 25, 2017 to 31 January 31, 2017 in Beijing, the vertical aerosol mass flux varied substantially during the different stages. Specifically, the mean mass flux decreased by 51% from 0.0049 mg m<sup>-2</sup>s<sup>-1</sup> in the RSs to 0.0024 mg m<sup>-2</sup>s<sup>-1</sup> in the TSs, which was partly due to the wind speed reduction from strong northerly winds in the RSs to southerly winds in the TSs. During the ASs, the mean mass flux decreased further to 0.00087 mg m<sup>-2</sup>s<sup>-1</sup>, which accounted for approximately 1/3 of the flux during the TSs. ~~Due to the cooling effect of elevated aerosols in the ASs, the near-ground temperature decreased and caused or reinforced the inversion, which suppressed the turbulence diffusion.~~ The weakened mass flux would further facilitate aerosol accumulation. During the HPE from December 01, 2016, to December 22, 2016, in Gucheng, the mean mass flux was similar in the RSs and TSs, ranging from 0.00063 mg m<sup>-2</sup>s<sup>-1</sup> to 0.00065 mg m<sup>-2</sup>s<sup>-1</sup>. This is partly because Gucheng was less affected by strong northerly winds than Beijing. Thus, the wind speed varied slightly from the RSs to TSs. However, the mass flux decreased substantially to 0.00025 mg m<sup>-2</sup>s<sup>-1</sup> in the ASs, which was merely 1/3 of the mean flux in the TSs.

~~Based on our measurement results, it can be seen that from the TS to the AS, the aerosol vertical turbulent flux decreased, but the aerosol particle concentration with surface layer increased. it is inferred that in addition to the contribution of regional transport from upwind areas during the TS, suppression of vertical turbulence mixing confining aerosols to a shallow boundary layer increased accumulation.~~

In this study, the aerosol emission flux was also estimated in these two rural and urban sites. Generally, compared with the emissions in spring, we found that in winter, the near-ground emissions were weaker in suburban areas and were similar in urban areas. In suburban areas, although the aerosol concentrations were relatively high (Shen et al., 2018)(Shen et al., 2018), the upward emitted aerosol flux was smaller than in urban areas. During the ASs of the HPEs, the aerosol emission flux from the ground was weaker than for the RSs and TSs at both the CAMS and GC sites, which indicates that surface pollutant emissions are not the major cause of explosive PM<sub>2.5</sub> growth. During the ASs with weak solar radiation, the factors most associated with aerosol concentration changes were horizontal transport and BL height variations, which might be the ~~main~~ causes of increased PM<sub>2.5</sub> (Zhong et al., 2018b; Zhong et al., 2018a; Zhang et al., 2018) leading causes of increased PM<sub>2.5</sub>. This is in line with previous studies that the main reason for the explosive growth of aerosol concentration during AS is attributed to the horizontal transport during TS. The TS will definitely appear before CS. The south or southwest wind will always appear in the TS, and the concentration of PM<sub>10</sub> in Baoding is higher than the mass of PM<sub>10</sub> in Beijing, which is generally maintained for one to two days. Except for the southerly or southwesterly winds for one to two days, there will be no CS in Beijing. Even if it is a southerly or southwesterly wind, if the wind speed is too small (<1 ms<sup>-1</sup>), AS will not appear. Only the southerly or southwesterly wind with a wind speed

带格式的: 字体颜色: 自动设置

greater than a specific value ( $>1.5 \text{ m s}^{-1}$ ), and the concentration of  $\text{PM}_{10}$  in the area to the south of Beijing is higher than that in Beijing, and then there will be CS after a small wind (Zhong et al., 2018c; Zhong et al., 2018b; Zhang et al., 2018).

Compared to the results (Yuan et al. 2016) from Hefei, China, a small and medium-sized provincial capital city in East China, the measured aerosol mass-fluxes in Beijing are almost at the same amount. A series of measures and actions have been made for emission reduction in Beijing, and the main emission is from vehicles. The difference in aerosol mass flux may be small.

Due to the lack of necessary experimental conditions, such as meteorological towers and EC systems, current experimental results cannot be compared with EC methods. According to the literature data, the two methods have been compared indirectly, and the estimated aerosol flux under different measurement conditions is consistent in magnitude (Yuan et al., 2016)(Yuan et al., 2016). However, a direct comparison of the two methods is in development.

Compared with the EC method, the aerosol flux has high spatial representativeness based on the principle of light propagation, and there is no need to install a hightall tower. However, the estimation of aerosol fluxes using the LAS method still has theoretical and practical deficiencies. At present, the LAS method for the aerosol flux regards the aerosol particles as ordinary scalar molecules. At the same time, based on the assumption of the equivalent medium, the imaginary part of the AERI is taken for granted as proportional to the aerosol mass concentration. This is often not the case. The actual turbulence spectrum shape ~~often deviates~~may deviate from the " $5/3$ " law von Karman spectrum, and turbulence intermittent and scintillation saturation can also occur (Moene et al., 2009)(Moene et al., 2009). The applicability of the near-surface layer similarity theory to the aerosol particle motion under stable layer conditions also has many problems. The formation of new particles and changes in aerosol particle size distribution also affect the scintillation in light propagation. There are also practical problems such as untimely maintenance, rainfall and low visibility, and platform vibrations required for observation. All these problems will cause errors in final estimates, so more theoretical and experimental research is needed.

**Author contributions.** Renmin Yuan and Xiaoye Zhang designed experiments and wrote the manuscript; Renmin Yuan, Hao Liu, Yu Gui, Bohao Shao, Yaqiang Wang, Junting Zhong and Xiaoping Tao carried out experiments; Renmin Yuan analyzed experimental results. Yubin Li and Zhiqiu Gao designed experiments and discussed the results.

**Acknowledgements.** This study was supported by the National Key Research and Development Program under grant no. 2016YFC0203306 and the National Natural Science Foundation of China (41775014, 51677175). We also thank two anonymous reviewers for their constructive and helpful comments.

## References

- Ahlm, L., Krejci, R., Nilsson, E. D., Martensson, E. M., Vogt, M., and Artaxo, P.: Emission and dry deposition of accumulation mode particles in the Amazon Basin, Atmospheric Chemistry And Physics, 10, 10237-10253, 10.5194/acp-10-10237-2010, 2010a.
- Ahlm, L., Nilsson, E. D., Krejci, R., Martensson, E. M., Vogt, M., and Artaxo, P.: A comparison of dry and wet season aerosol number fluxes over the Amazon rain forest, Atmospheric Chemistry And Physics, 10, 3063-3079, 10.5194/acp-10-3063-2010, 2010b.

带格式的: 字体颜色: 自动设置

带格式的: 缩进: 左侧: 0 厘米, 悬挂缩进: 2 字符, 首行缩进: -2 字符

- Akagi, S. K., Yokelson, R. J., Wiedinmyer, C., Alvarado, M. J., Reid, J. S., Karl, T., Crounse, J. D., and Wennberg, P. O.: Emission factors for open and domestic biomass burning for use in atmospheric models, *Atmospheric Chemistry And Physics*, 11, 4039-4072, 10.5194/acp-11-4039-2011, 2011.
- Bond, T. C., Streets, D. G., Yarber, K. F., Nelson, S. M., Woo, J. H., and Klimont, Z.: A technology-based global inventory of black and organic carbon emissions from combustion, *Journal Of Geophysical Research-Atmospheres*, 109, 10.1029/2003jd003697, 2004.
- [Brion, J., Chakir, A., Charbonnier, J., Daumont, D., Parisse, C., and Malicet, J.: Absorption spectra measurements for the ozone molecule in the 350-830 nm region, \*J. Atmos. Chem.\*, 30, 291-299, 10.1023/a:1006036924364, 1998.](#)
- Brooks, I. M., Yelland, M. J., Upstill-Goddard, R. C., Nightingale, P. D., Archer, S., d'Asaro, E., Beale, R., Beatty, C., Blomquist, B., Bloom, A. A., Brooks, B. J., Cludray, J., Coles, D., Dacey, J., DeGrandpre, M., Dixon, J., Drennan, W. M., Gabriele, J., Goldson, L., Hardman-Mountford, N., Hill, M. K., Horn, M., Hsueh, P.-C., Huebert, B., de Leeuw, G., Leighton, T. G., Liddicoat, M., Lingard, J. J. N., McNeil, C., McQuaid, J. B., Moat, B. I., Moore, G., Neill, C., Norris, S. J., O'Doherty, S., Pascal, R. W., Prytherch, J., Rebozo, M., Sahlee, E., Salter, M., Schuster, U., Skjelvan, I., Slagter, H., Smith, M. H., Smith, P. D., Srokosz, M., Stephens, J. A., Taylor, P. K., Telszewski, M., Walsh, R., Ward, B., Woolf, D. K., Young, D., and Zimmelink, H.: Physical exchanges at the air-sea interface uk-solas field measurements, *Bulletin of the American Meteorological Society*, 90, 629+, 10.1175/2008bams2578.1, 2009.
- [Buzorius, G., Rannik, U., Makela, J. M., Vesala, T., and Kulmala, M.: Vertical aerosol particle fluxes measured by eddy covariance technique using condensational particle counter. \*Journal of Aerosol Science\*, 29, 157-171, 10.1016/s0021-8502\(97\)00458-8, 1998.](#)
- Cao, J., Xu, H., Xu, Q., Chen, B., and Kan, H.: Fine Particulate Matter Constituents and Cardiopulmonary Mortality in a Heavily Polluted Chinese City, *Environmental Health Perspectives*, 120, 373-378, 10.1289/ehp.1103671, 2012.
- Ceburnis, D., Rinaldi, M., Ovadnevaite, J., Martucci, G., Giulianelli, L., and O'Dowd, C. D.: Marine submicron aerosol gradients, sources and sinks, *Atmospheric Chemistry and Physics*, 16, 12425-12439, 10.5194/acp-16-12425-2016, 2016.
- Chen, Y., Tian, C., Feng, Y., Zhi, G., Li, J., and Zhang, G.: Measurements of emission factors of PM<sub>2.5</sub>, OC, EC, and BC for household stoves of coal combustion in China, *Atmospheric Environment*, 109, 190-196, 10.1016/j.atmosenv.2015.03.023, 2015.
- Cheng, Y. G., and Brutsaert, W.: Flux-profile relationships for wind speed and temperature in the stable atmospheric boundary layer, *Boundary-Layer Meteorology*, 114, 519-538, 10.1007/s10546-004-1425-4, 2005.
- DeBruin, H. A. R., vandenHurk, B., and Kohsiek, W.: The scintillation method tested over a dry vineyard area, *Boundary-Layer Meteorology*, 76, 25-40, 1995.
- Dou, J., Wang, Y., and Miao, S.: Fine Spatial and Temporal Characteristics of Humidity and Wind in Beijing Urban Area, *Journal of Applied Meteorological Science*, 25, 559-569, 2014.
- Dubovik, O., Holben, B., Eck, T. F., Smirnov, A., Kaufman, Y. J., King, M. D., Tanre, D., and Slutsker, I.: Variability of absorption and optical properties of key aerosol types observed in worldwide locations, *J. Atmos. Sci.*, 59, 590-608, 10.1175/1520-0469(2002)059<0590:voaaop>2.0.co;2, 2002.
- Elbert, W., Taylor, P. E., Andreae, M. O., and Poeschl, U.: Contribution of fungi to primary biogenic aerosols in the atmosphere: wet and dry discharged spores, carbohydrates, and inorganic ions, *Atmospheric Chemistry and Physics*, 7, 4569-4588, 10.5194/acp-7-4569-2007, 2007.
- EPD, E. P. D.: Technical regulation on ambient air quality index (on trial), Beijing, 12 pp., 2012.
- Evans, J. G., and De Bruin, H. A. R.: The Effective Height of a Two-Wavelength Scintillometer System, *Bound-Lay.*

带格式的: 缩进: 左侧: 0 厘米, 悬挂缩进: 2 字符, 首行缩进: -2 字符

带格式的: 缩进: 左侧: 0 厘米, 悬挂缩进: 2 字符, 首行缩进: -2 字符

773 Meteorol., 141, 165-177, 10.1007/s10546-011-9634-0, 2011.

774 Farmer, D. K., Kimmel, J. R., Phillips, G., Docherty, K. S., Worsnop, D. R., Sueper, D., Nemitz, E., and Jimenez, J.  
775 L.: Eddy covariance measurements with high-resolution time-of-flight aerosol mass spectrometry: a new  
776 approach to chemically resolved aerosol fluxes, *Atmos. Meas. Tech.*, 4, 1275-1289, 10.5194/amt-4-1275-2011,  
777 2011.

778 Gordon, M., Staebler, R. M., Liggio, J., Vlasenko, A., Li, S.-M., and Hayden, K.: Aerosol flux measurements above  
779 a mixed forest at Borden, Ontario *Atmos. Chem. Phys.*, 11, 6773-6786, 2011.

780 Graham, B., Guyon, P., Taylor, P. E., Artaxo, P., Maenhaut, W., Glovsky, M. M., Flagan, R. C., and Andreae, M. O.:  
781 Organic compounds present in the natural Amazonian aerosol: Characterization by gas chromatography-mass  
782 spectrometry, *Journal Of Geophysical Research-Atmospheres*, 108, 10.1029/2003jd003990, 2003.

783 Guo, H., Xu, M., and Hu, Q.: Changes in near-surface wind speed in China: 1969-2005, *International Journal Of*  
784 *Climatology*, 31, 349-358, 10.1002/joc.2091, 2011.

785 [Guo, S., Hu, M., Zamora, M. L., Peng, J. F., Shang, D. J., Zheng, J., Du, Z. F., Wu, Z., Shao, M., Zeng, L. M., Molina,](#)  
786 [M. J., and Zhang, R. Y.: Elucidating severe urban haze formation in China, \*Proc. Natl. Acad. Sci. U.S.A.\*, 111,](#)  
787 [17373-17378, 10.1073/pnas.1419604111, 2014.](#)

788 Harrison, R. M., Dall'Osto, M., Beddows, D. C. S., Thorpe, A. J., Bloss, W. J., Allan, J. D., Coe, H., Dorsey, J. R.,  
789 Gallagher, M., Martin, C., Whitehead, J., Williams, P. I., Jones, R. L., Langridge, J. M., Benton, A. K., Ball, S.  
790 M., Langford, B., Hewitt, C. N., Davison, B., Martin, D., Petersson, K. F., Henshaw, S. J., White, I. R.,  
791 Shallcross, D. E., Barlow, J. F., Dunbar, T., Davies, F., Nemitz, E., Phillips, G. J., Helfter, C., Di Marco, C. F.,  
792 and Smith, S.: Atmospheric chemistry and physics in the atmosphere of a developed megacity (London): an  
793 overview of the REPARTEE experiment and its conclusions, , *Atmos. Chem. Phys.*, 12, 3065-3114,  
794 10.5194/acp-12-3065-2012, 2012, 2012.

795 Hartogensis, O. K., Watts, C. J., Rodriguez, J. C., and De Bruin, H. A. R.: Derivation of an effective height for  
796 scintillometers: La Poza experiment in Northwest Mexico, *Journal of Hydrometeorology*, 4, 915-928,  
797 10.1175/1525-7541(2003)004<0915:doahf>2.0.co;2, 2003.

798 He, Y., Gao, Z., Guo, T., Qu, F., Liang, D., Li, D., Shi, J., and Shan, B.: Fine particulate matter associated mortality  
799 burden of lung cancer in Hebei Province, China, *Thoracic Cancer*, 9, 820-826, 10.1111/1759-7714.12653, 2018.

800 Hourdin, F., Gueye, M., Diallo, B., Dufresne, J. L., Escribano, J., Menut, L., Marticorena, B., Siour, G., and Guichard,  
801 F.: Parameterization of convective transport in the boundary layer and its impact on the representation of the  
802 diurnal cycle of wind and dust emissions, *Atmospheric Chemistry and Physics*, 15, 6775-6788, 10.5194/acp-  
803 15-6775-2015, 2015.

804 Huang, R.-J., Zhang, Y., Bozzetti, C., Ho, K.-F., Cao, J.-J., Han, Y., Daellenbach, K. R., Slowik, J. G., Platt, S. M.,  
805 Canonaco, F., Zotter, P., Wolf, R., Pieber, S. M., Bruns, E. A., Crippa, M., Ciarelli, G., Piazzalunga, A.,  
806 Schwikowski, M., Abbaszade, G., Schnelle-Kreis, J., Zimmermann, R., An, Z., Szidat, S., Baltensperger, U., El  
807 Haddad, I., and Prevot, A. S. H.: High secondary aerosol contribution to particulate pollution during haze events  
808 in China, *Nature*, 514, 218-222, 10.1038/nature13774, 2014.

809 Jarvi, L., Rannik, U., Mammarella, I., Sogachev, A., Aalto, P. P., Keronen, P., Siivola, E., Kulmala, M., and Vesala,  
810 T.: Annual particle flux observations over a heterogeneous urban area, *Atmos. Chem. Phys.*, 9, 7847-7856,  
811 2009.

812 Kaimal, J. C., Izumi, Y., Wyngaard, J. C., and Cote, R.: Spectral characteristics of surface-layer turbulence, *Q. J.*  
813 *Roy. Meteor. Soc.*, 98, 563-589, 1972.

814 Karvosenoja, N., Tainio, M., Kupiainen, K., Tuomisto, J. T., Kukkonen, J., and Johansson, M.: Evaluation of the  
815 emissions and uncertainties of PM2.5 originated from vehicular traffic and domestic wood combustion in  
816 Finland, *Boreal Environment Research*, 13, 465-474, 2008.

带格式的: 缩进: 左侧: 0 厘米, 悬挂缩进: 2 字符,  
首行缩进: -2 字符



- Ketzel, M., Wahlin, P., Berkowicz, R., and Palmgren, F.: Particle and trace gas emission factors under urban driving conditions in Copenhagen based on street and roof-level observations, *Atmospheric Environment*, 37, 2735-2749, 10.1016/s1352-2310(03)00245-0, 2003.
- Krecl, P., Targino, A. C., Landi, T. P., and Ketzel, M.: Determination of black carbon, PM<sub>2.5</sub>, particle number and NO<sub>x</sub> emission factors from roadside measurements and their implications for emission inventory development, *Atmospheric Environment*, 186, 229-240, 10.1016/j.atmosenv.2018.05.042, 2018.
- Lagouarde, J. P., Irvine, M., Bonnefond, J. M., Grimmond, C. S. B., Long, N., Oke, T. R., Salmond, J. A., and Offerle, B.: Monitoring the sensible heat flux over urban areas using large aperture scintillometry: Case study of Marseille city during the escompte experiment, *Boundary-Layer Meteorology*, 118, 449-476, 10.1007/s10546-005-9001-0, 2006.
- Leclerc, M. Y., and Foken, T.: *Footprints in Micrometeorology and Ecology*, Springer, Heidelberg, 254 pp., 2014.
- Lee, X.: *Handbook of Micrometeorology, A Guide for Surface Flux Measurement and Analysis*, edited by: Lee, X., Kluwer academic publishers, New York, USA, 250 pp., 2004.
- Lei, H., and Wuebbles, D. J.: Chemical competition in nitrate and sulfate formations and its effect on air quality, *Atmospheric Environment*, 80, 472-477, 10.1016/j.atmosenv.2013.08.036, 2013.
- Li, J., Sun, J., Zhou, M., Cheng, Z., Li, Q., Cao, X., and Zhang, J.: Observational analyses of dramatic developments of a severe air pollution event in the Beijing area, *Atmospheric Chemistry and Physics*, 18, 3919-3935, 10.5194/acp-18-3919-2018, 2018.
- Li, M., Liu, H., Geng, G., Hong, C., Liu, F., Song, Y., Tong, D., Zheng, B., Cui, H., Man, H., Zhang, Q., and He, K.: [Anthropogenic emission inventories in China: a review, National Science Review, 4, 834-866, 10.1093/nsr/nwx150, 2017.](#)
- Li, Q.-c., Li, J., Zheng, Z.-f., Wang, Y.-t., and Yu, M.: [Influence of mountain valley breeze and sea land breeze in winter on distribution of air pollutants in beijing-tianjin-hebei region, Environmental Science & Technology, 40, 513-524, 2019.](#)
- Li, X., Hu, F., and Shu, W.: Study on the characteristics of winter island heat islands in Beijing and the influence factors of strong and weak heat islands, *Journal of the Graduate School of the Chinese Academy of Sciences*, 4, 431-438, 2007.
- Liu, H., Man, H., Cui, H., Wang, Y., Deng, F., Wang, Y., Yang, X., Xiao, Q., Zhang, Q., Ding, Y., and He, K.: An updated emission inventory of vehicular VOCs and IVOCs in China, *Atmospheric Chemistry And Physics*, 17, 12709-12724, 10.5194/acp-17-12709-2017, 2017.
- Lou, S., Liao, H., and Zhu, B.: [Impacts of aerosols on surface-layer ozone concentrations in China through heterogeneous reactions and changes in photolysis rates, Atmos. Environ., 85, 123-138, 10.1016/j.atmosenv.2013.12.004, 2014.](#)
- Lu, Z., Zhang, Q., and Streets, D. G.: Sulfur dioxide and primary carbonaceous aerosol emissions in China and India, 1996-2010, *Atmospheric Chemistry And Physics*, 11, 9839-9864, 10.5194/acp-11-9839-2011, 2011.
- Martensson, E. M., Nilsson, E. D., Buzorius, G., and Johansson, C.: Eddy covariance measurements and parameterisation of traffic related particle emissions in an urban environment, *Atmos. Chem. Phys.*, 6, 769-785, 2006.
- Mayol, E., Jimenez, M. A., Herndl, G. J., Duarte, C. M., and Arrieta, J. M.: Resolving the abundance and air-sea fluxes of airborne microorganisms in the North Atlantic Ocean, *Frontiers in Microbiology*, 5, 10.3389/fmicb.2014.00557, 2014.
- MEP, P. R. C.: *Technical regulation on ambient air quality index*, Ministry of Environmental Protection, Beijing, 12 pp., 2012.
- Moene, A. F., Beyrich, F., and Hartogensis, O. K.: Developments in scintillometry, *Bulletin of the American*

带格式的: 缩进: 左侧: 0 厘米, 悬挂缩进: 2 字符, 首行缩进: -2 字符

带格式的: 缩进: 左侧: 0 厘米, 悬挂缩进: 2 字符, 首行缩进: -2 字符



861 Meteorological Society, 90, 694-698, 10.1175/2008bams2672.1, 2009.

862 [Nebuloni, R.: Empirical relationships between extinction coefficient and visibility in fog, Appl. Opt., 44, 3795-3804,](#)

863 [10.1364/ao.44.003795, 2005.](#)

864 Nemitz, E., Dorsey, J. R., Flynn, M. J., Gallagher, M. W., Hensen, A., Erisman, J.-W., Owen, S. M., amngen, U. D.,

865 and Sutton, M. A.: Aerosol fluxes and particle growth above managed grassland, Biogeosciences, 6, 1627-1645,

866 2009.

867 Ripamonti, G., Jarvi, L., Molgaard, B., Hussein, T., Nordbo, A., and Hameri, K.: The effect of local sources on

868 aerosol particle number size distribution, concentrations and fluxes in Helsinki, Finland, Tellus B., 65,

869 10.3402/tellusb.v65i0.19786, 2013.

870 Roden, C. A., Bond, T. C., Conway, S., Benjamin, A., and Pinel, O.: Emission factors and real-time optical properties

871 of particles emitted from traditional wood burning cookstoves, Environmental Science & Technology, 40, 6750-

872 6757, 10.1021/es052080i, 2006.

873 Shen, G., Tao, S., Wei, S., Chen, Y., Zhang, Y., Shen, H., Huang, Y., Zhu, D., Yuan, C., Wang, H., Wang, Y., Pei, L.,

874 Liao, Y., Duan, Y., Wang, B., Wang, R., Lv, Y., Li, W., Wang, X., and Zheng, X.: Field Measurement of Emission

875 Factors of PM, EC, OC, Parent, Nitro-, and Oxy- Polycyclic Aromatic Hydrocarbons for Residential Briquette,

876 Coal Cake, and Wood in Rural Shanxi, China, Environmental Science & Technology, 47, 2998-3005,

877 10.1021/es304599g, 2013.

878 Shen, X., Sun, J., Zhang, X., Zhang, Y., Wang, Y., Tan, K., Wang, P., Zhang, L., Qi, X., Che, H., Zhang, Z., Zhong,

879 J., Zhao, H., and Ren, S.: Comparison of Submicron Particles at a Rural and an Urban Site in the North China

880 Plain during the December 2016 Heavy Pollution Episodes, Journal of Meteorological Research, 32, 26-37,

881 10.1007/s13351-018-7060-7, 2018.

882 Sproson, D. A. J., Brooks, I. M., and Norris, S. J.: The effect of hygroscopicity on eddy covariance estimates of sea-

883 spray aerosol fluxes: a comparison of high-rate and bulk correction methods, Atmos. Meas. Tech., 6, 323-335,

884 2013.

885 Stull, R. B.: An Introduction to Boundary Layer Meteorology, Reidel Publishing Co., Dordrecht, 666 pp., 1988.

886 [Su, F., Gao, Q., Zhang, Z., REN, Z.-h., and YANG, X.-x.: Transport pathways of pollutants from outside in](#)

887 [atmosphere boundary layer, Res. Environ. Sci., 1, 26-29, 10.13198/j.res.2004.01.28.sufq.005, 2004.](#)

888 Sun, Y., Jiang, Q., Wang, Z., Fu, P., Li, J., Yang, T., and Yin, Y.: Investigation of the sources and evolution processes

889 of severe haze pollution in Beijing in January 2013, Journal Of Geophysical Research-Atmospheres, 119, 4380-

890 4398, 10.1002/2014jd021641, 2014.

891 Tatarskii, V. I.: Wave Propagation in a Turbulent Medium, McGraw-Hill Book Company Inc., New York, 285 pp.,

892 1961.

893 Vogt, M., Nilsson, E. D., Ahlm, L., Martensson, E. M., and Johansson, C.: Seasonal and diurnal cycles of 0.25-2.5

894  $\mu\text{m}$  aerosol fluxes over urban Stockholm, Sweden, Tellus B., 63, 935-951, 10.1111/j.1600-0889.2011.00551.x,

895 2011a.

896 Vogt, M., Nilsson, E. D., Ahlm, L., Martensson, E. M., and Johansson, C.: The relationship between 0.25-2.5  $\mu\text{m}$

897 aerosol and CO<sub>2</sub> emissions over a city, Atmos. Chem. Phys., 11, 4851-4859, 10.5194/acp-11-4851-2011, 2011b.

898 Wang, H., Lu, K., Chen, X., Zhu, Q., Wu, Z., Wu, Y., and Sun, K.: Fast particulate nitrate formation via N<sub>2</sub>O<sub>5</sub> uptake

899 aloft in winter in Beijing, Atmospheric Chemistry and Physics, 18, 10483-10495, 10.5194/acp-18-10483-2018,

900 2018.

901 Wang, Y. H., Liu, Z. R., Zhang, J. K., Hu, B., Ji, D. S., Yu, Y. C., and Wang, Y. S.: Aerosol physicochemical properties

902 and implications for visibility during an intense haze episode during winter in Beijing, Atmospheric Chemistry

903 And Physics, 15, 3205-3215, 10.5194/acp-15-3205-2015, 2015.

904 Wang, Z., Li, J., Wang, Z., Yang, W., Tang, X., Ge, B., Yan, P., Zhu, L., Chen, X., Chen, H., Wand, W., Li, J., Liu,

带格式的: 缩进: 左侧: 0 厘米, 悬挂缩进: 2 字符,  
首行缩进: -2 字符

带格式的: 缩进: 左侧: 0 厘米, 悬挂缩进: 2 字符,  
首行缩进: -2 字符

---

B., Wang, X., Wand, W., Zhao, Y., Lu, N., and Su, D.: Modeling study of regional severe hazes over mid-eastern China in January 2013 and its implications on pollution prevention and control, *Science China-Earth Sciences*, 57, 3-13, 10.1007/s11430-013-4793-0, 2014.

Whitehead, J. D., Gallagher, M. W., Dorsey, J. R., Robinson, N., Gabey, A. M., Coe, H., McFiggans, G., Flynn, M. J., Ryder, J., Nemitz, E., and Davies, F.: Aerosol fluxes and dynamics within and above a tropical rainforest in South-East Asia, *Atmospheric Chemistry and Physics*, 10, 9369-9382, 10.5194/acp-10-9369-2010, 2010.

Wu, Q., Wang, Z., Chen, H., Zhou, W., and Wenig, M.: An evaluation of air quality modeling over the Pearl River Delta during November 2006, *Meteorology And Atmospheric Physics*, 116, 113-132, 10.1007/s00703-011-0179-z, 2012.

Wyngaard, J. C., Izumi, Y., and Collins, S. A.: Behavior of refractive-index-structure parameter near ground, *J. Opt. Soc. Am.*, 61, 1646-1650, 10.1364/josa.61.001646, 1971.

Wyngaard, J. C.: *Turbulence in the Atmosphere*, Cambridge University Press, New York, 393 pp., 2010.

Yuan, R., Luo, T., Sun, J., Zeng, Z., Ge, C., and Fu, Y.: A new method for measuring the imaginary part of the atmospheric refractive index structure parameter in the urban surface layer, *Atmospheric Chemistry and Physics*, 15, 2521-2531, 10.5194/acp-15-2521-2015, 2015.

Yuan, R., Luo, T., Sun, J., Liu, H., Fu, Y., and Wang, Z.: A new method for estimating aerosol mass flux in the urban surface layer using LAS technology, *Atmospheric Measurement Techniques*, 9, 1925-1937, 10.5194/amt-9-1925-2016, 2016.

Zeweldi, D. A., Gebremichael, M., Wang, J., Sammis, T., Kleissl, J., and Miller, D.: Intercomparison of Sensible Heat Flux from Large Aperture Scintillometer and Eddy Covariance Methods: Field Experiment over a Homogeneous Semi-arid Region, *Bound-Lay. Meteorol.*, 135, 151-159, 10.1007/s10546-009-9460-9, 2010.

Zhang, H., and Li, X.: Review of the field measurements and parameterization for dust emission during sand-dust events, *Journal of Meteorological Research*, 28, 903-922, 10.1007/s13351-014-3296-z, 2014.

Zhang, Q., Streets, D. G., Carmichael, G. R., He, K. B., Huo, H., Kannari, A., Klimont, Z., Park, I. S., Reddy, S., Fu, J. S., Chen, D., Duan, L., Lei, Y., Wang, L. T., and Yao, Z. L.: Asian emissions in 2006 for the NASA INTEX-B mission, *Atmospheric Chemistry And Physics*, 9, 5131-5153, 10.5194/acp-9-5131-2009, 2009a.

Zhang, X., Zhong, J., Wang, J., Wang, Y., and Liu, Y.: The interdecadal worsening of weather conditions affecting aerosol pollution in the Beijing area in relation to climate warming, *Atmospheric Chemistry and Physics*, 18, 5991-5999, 10.5194/acp-18-5991-2018, 2018.

Zhang, X. Y., Wang, Y. Q., Lin, W. L., Zhang, Y. M., Zhang, X. C., Gong, S., Zhao, P., Yang, Y. Q., Wang, J. Z., Hou, Q., Zhang, X. L., Che, H. Z., Guo, J. P., and Li, Y.: CHANGES OF ATMOSPHERIC COMPOSITION AND OPTICAL PROPERTIES OVER BEIJING 2008 Olympic Monitoring Campaign, *Bulletin Of the American Meteorological Society*, 90, 1633-+, 10.1175/2009bams2804.1, 2009b.

Zhang, X. Y., Wang, Y. Q., Niu, T., Zhang, X. C., Gong, S. L., Zhang, Y. M., and Sun, J. Y.: Atmospheric aerosol compositions in China: spatial/temporal variability, chemical signature, regional haze distribution and comparisons with global aerosols, *Atmospheric Chemistry And Physics*, 12, 779-799, 10.5194/acp-12-779-2012, 2012.

Zhang, Y., and Tao, S.: Global atmospheric emission inventory of polycyclic aromatic hydrocarbons (PAHs) for 2004, *Atmospheric Environment*, 43, 812-819, 10.1016/j.atmosenv.2008.10.050, 2009.

Zheng, B., Zhang, Q., Tong, D., Chen, C., Hong, C., Li, M., Geng, G., Lei, Y., Huo, H., and He, K.: Resolution dependence of uncertainties in gridded emission inventories: a case study in Hebei, China, *Atmospheric Chemistry And Physics*, 17, 921-933, 10.5194/acp-17-921-2017, 2017.

Zhong, J., Zhang, X., Wang, Y., Sun, J., Zhang, Y., Wang, J., Tan, K., Shen, X., Che, H., and Zhang, L.: [Relative contributions of boundary-layer meteorological factors to the explosive growth of PM 2.5 during the red-alert](#)

heavy pollution episodes in Beijing in December 2016, *J. Meteorolog. Res.*, 31, 809-819, 10.1007/s13351-017-7088-0, 2017a.

Zhong, J., Zhang, X., Wang, Y., Sun, J., Zhang, Y., Wang, J., Tan, K., Shen, X., Che, H., Zhang, L., Zhang, Z., Qi, X., Zhao, H., Ren, S., and Li, Y.: Relative Contributions of Boundary-Layer Meteorological Factors to the Explosive Growth of PM<sub>2.5</sub> during the Red-Alert Heavy Pollution Episodes in Beijing in December 2016, *Journal Of Meteorological Research*, 31, 809-819, 10.1007/s13351-017-7088-0, 2017b.

Zhong, J., Zhang, X., Dong, Y., Wang, Y., Liu, C., Wang, J., Zhang, Y., and Che, H.: Feedback effects of boundary-layer meteorological factors on cumulative explosive growth of PM<sub>2.5</sub> during winter heavy pollution episodes in Beijing from 2013 to 2016, *Atmos. Chem. Phys.*, 18, 247-258, 10.5194/acp-18-247-2018, 2018a.

Zhong, J., Zhang, X., Dong, Y., Wang, Y., Liu, C., Wang, J., Zhang, Y., and Che, H.: Feedback effects of boundary-layer meteorological factors on cumulative explosive growth of PM<sub>2.5</sub> during winter heavy pollution episodes in Beijing from 2013 to 2016, *Atmospheric Chemistry And Physics*, 18, 247-258, 10.5194/acp-18-247-2018, 2018b.

Zhong, J., Zhang, X., Wang, Y., Liu, C., and Dong, Y.: Heavy aerosol pollution episodes in winter Beijing enhanced by radiative cooling effects of aerosols, *Atmospheric Research*, 209, 59-64, 10.1016/j.atmosres.2018.03.011, 2018c.

带格式的: 缩进: 左侧: 0 厘米, 悬挂缩进: 2 字符,  
首行缩进: -2 字符

带格式的: 缩进: 左侧: 0 厘米, 悬挂缩进: 2 字符,  
首行缩进: -2 字符

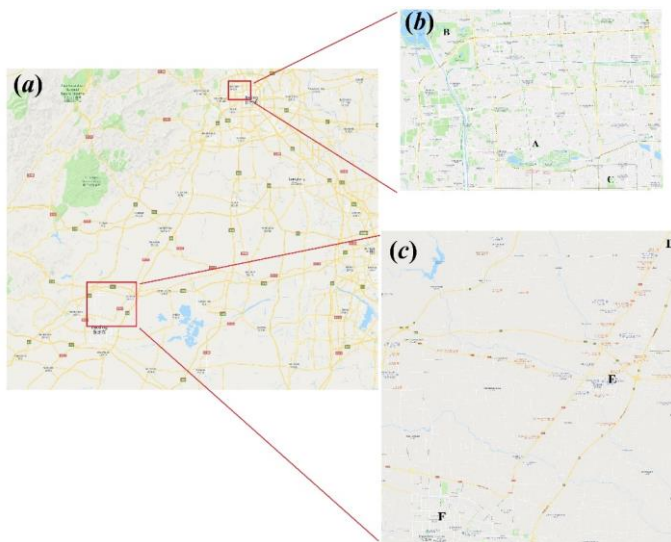


Figure 1. Photographs of the measurement site. (a) Map of the experiment area in the Beijing urban area and suburban area and (b) expanded view of the Beijing experiment area, which is marked as the shaded rectangle in (a). (c) Expanded view of the Baoding experiment area, which is marked as the shaded rectangle in (a). (d) Satellite image of the CAMS site and (e) the satellite image of the GC site. Figs. 1a, b, c, and d © Google.

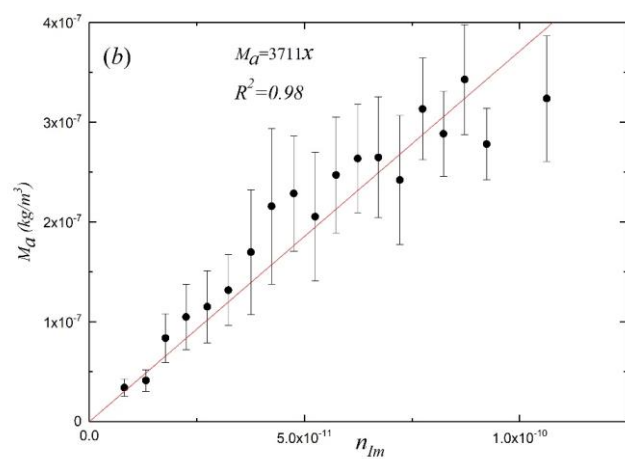
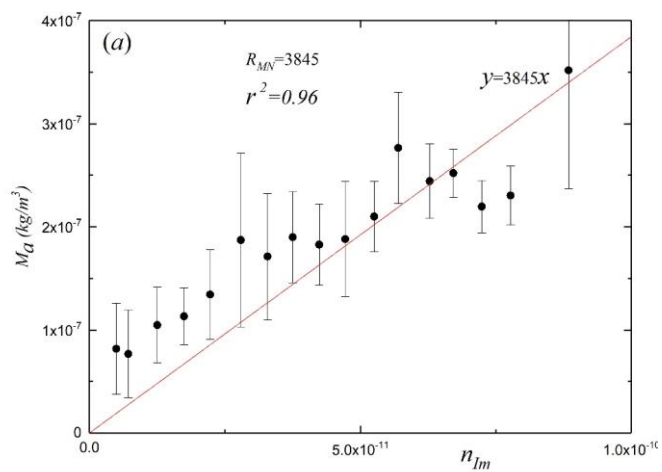


Figure 2. Scatterplots of aerosol mass concentration  $M_a$  vs. the imaginary part of the AERI for (a) the Beijing area and (b) the Baoding area.

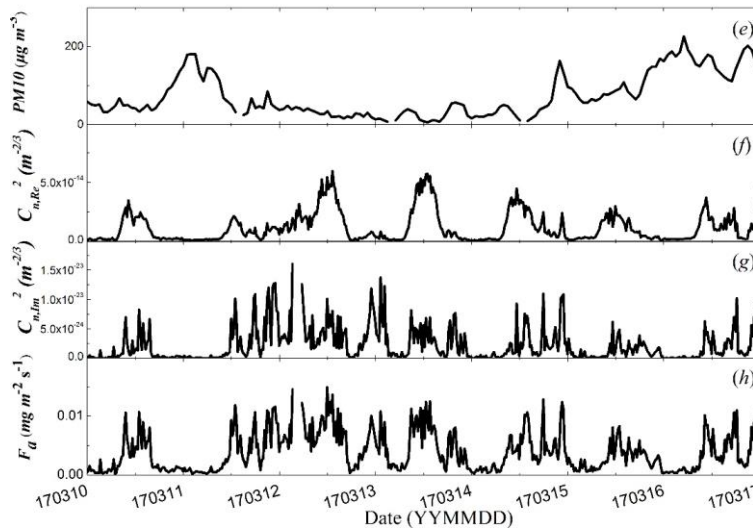
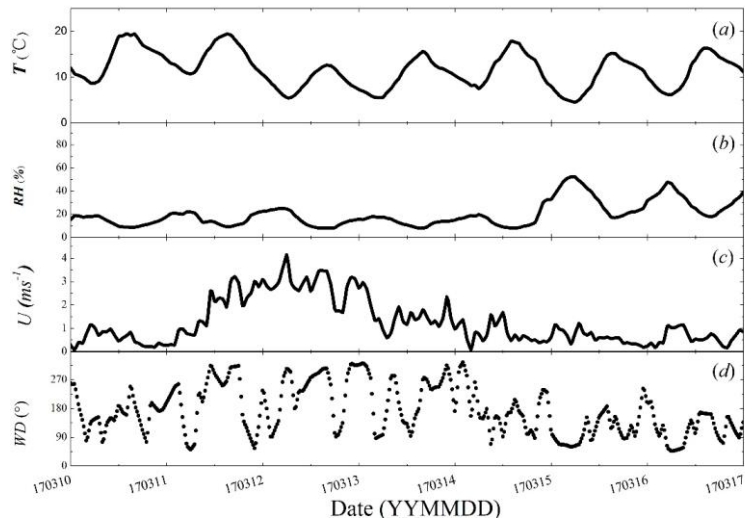


Figure 3. Temporal variations in (a) air temperature, (b) RH, (c) wind speed, (d) wind direction, (e)  $\text{PM}_{10}$ , (f) real part of the AERISP, (g) imaginary part of the AERISP and (h) aerosol mass flux in the Beijing area from March 10, 2017 to March 17, 2017.

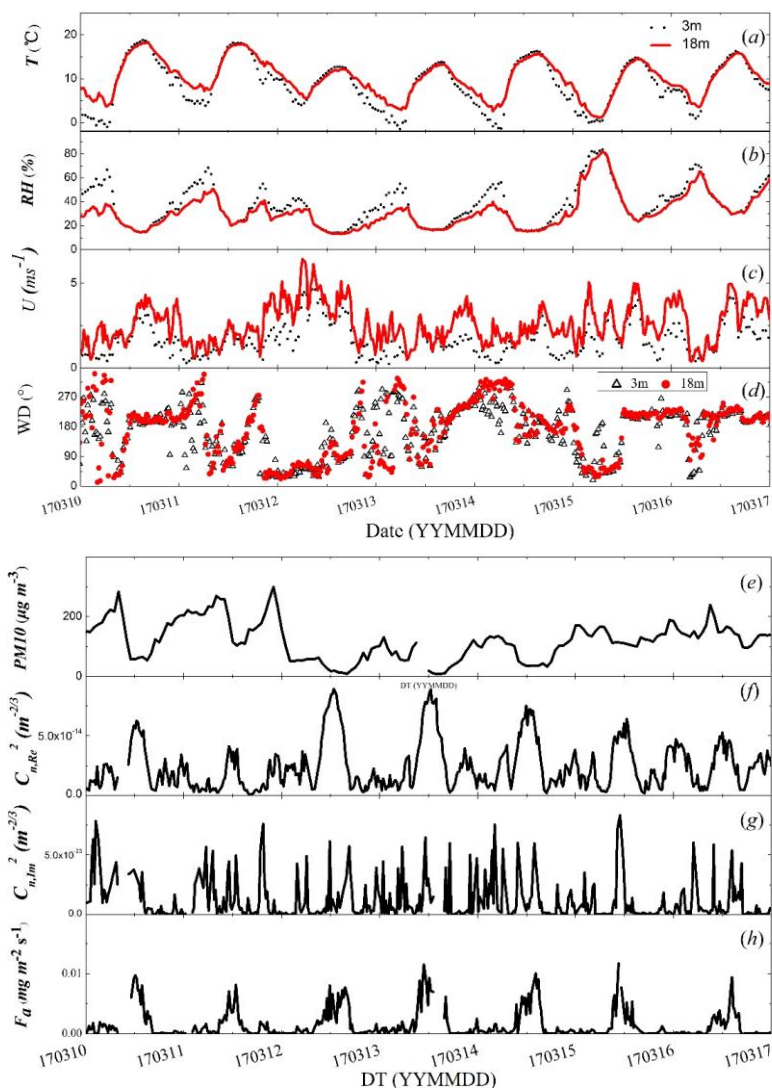
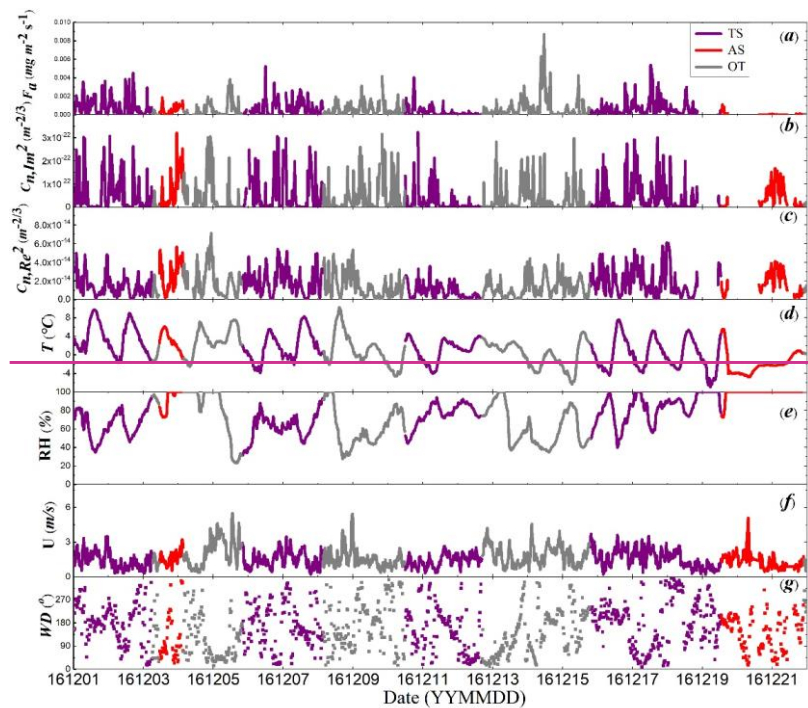


Figure 4. Temporal variations in (a) air temperature, (b) RH, (c) wind speed, (d) wind direction, (e) PM<sub>10</sub>, (f) real part of the AERISP, (g) imaginary part of the AERISP and (h) aerosol mass flux in the Baoding area from March 10, 2017 to March 17, 2017.





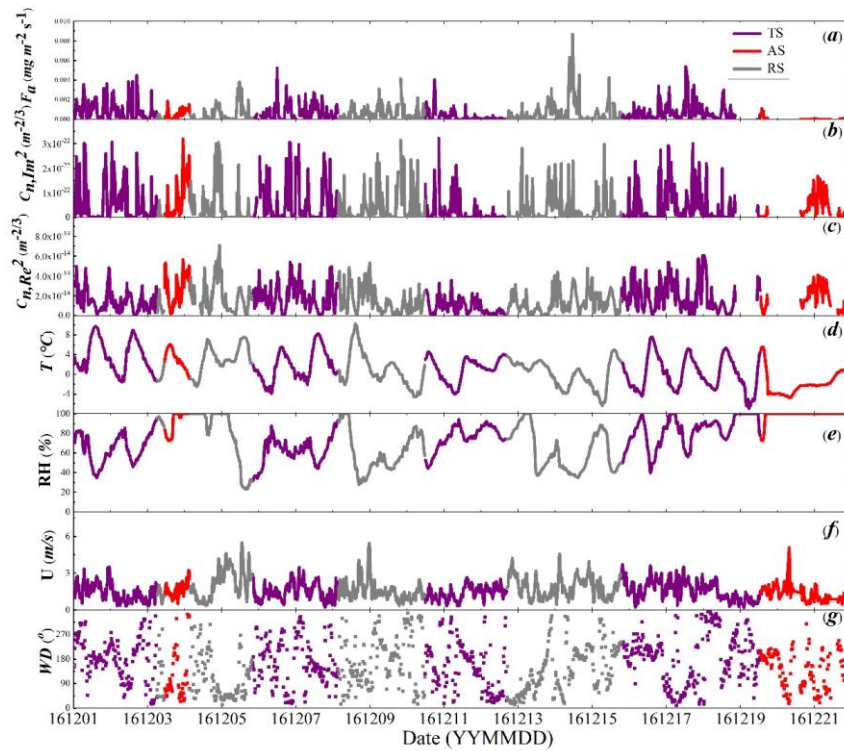
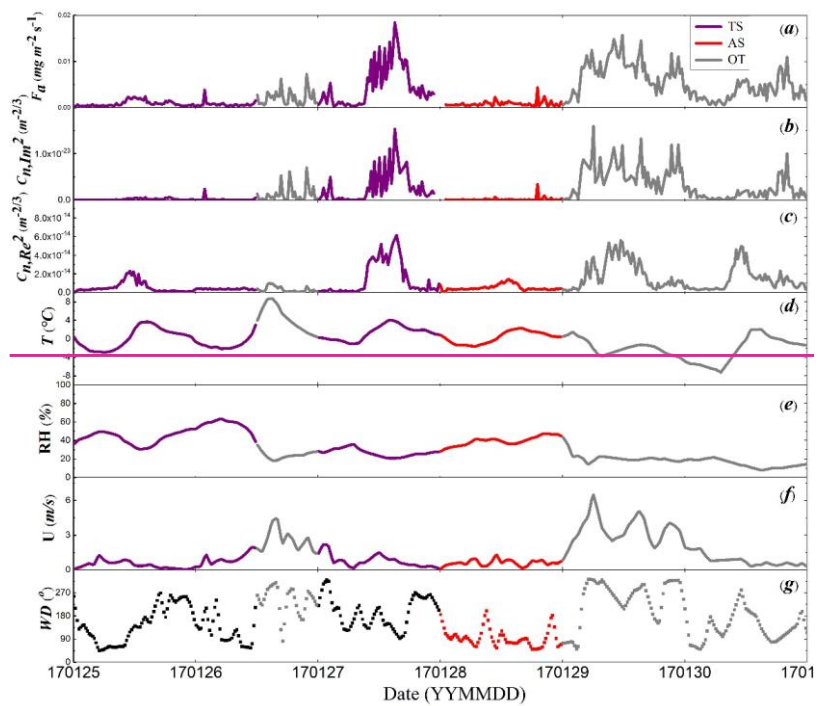


Figure 5. Temporal variations in (a) aerosol flux, (b) imaginary part of the AERISP, (c) real part of the AERISP (d) air temperature, (e) RH, (f) wind speed, and (g) wind direction in the Baoding area during a heavy pollution period, i.e., December 1, 2016 to December 22, 2016.



996

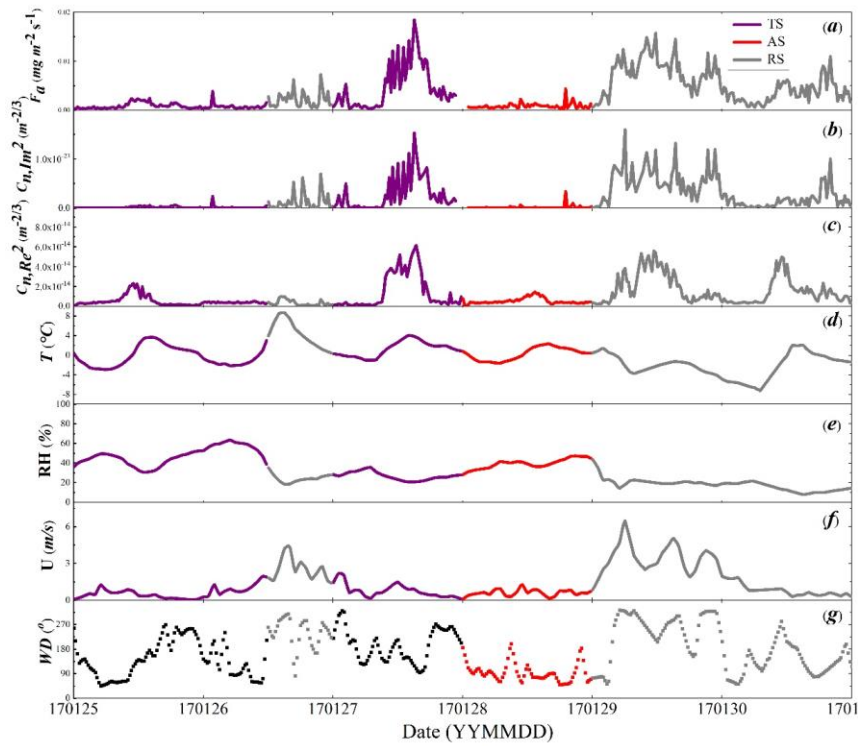


Figure 6. Temporal variations in (a) aerosol flux, (b) imaginary part of the AERISP, (c) real part of the AERISP (d) air temperature, (e) RH, (f) wind speed, and (g) wind direction in the Beijing area during a heavy pollution period, i.e., January 25, 2017 to January 31, 2017.